

# Is the low-energy optical absorption in correlated insulators controlled by quantum geometry?

Dan Mao,<sup>\*</sup> Juan Felipe Mendez-Valderrama,<sup>†</sup> and Debanjan Chowdhury<sup>‡</sup>  
*Department of Physics, Cornell University, Ithaca, New York 14853, USA.*

Inspired by the discovery of a variety of correlated insulators in the moiré universe, controlled by interactions projected to a set of isolated bands with a narrow bandwidth, we examine here a partial sum-rule associated with the inverse frequency-weighted optical conductivity restricted to low-energies. Unlike standard sum-rules that extend out to *infinite* frequencies, which include contributions from *all* inter-band transitions, we focus here on transitions associated *only* with the *projected* degrees of freedom. We analyze the partial sum-rule in a non-perturbative but “solvable” limit for a variety of correlation-induced insulators. This includes (i) magic-angle twisted bilayer graphene at integer-filling with projected Coulomb interactions, starting from the chiral flat-band limit and including realistic perturbations, (ii) fractional fillings of Chern-bands which support generalized Laughlin-like states, starting from a Landau-level and including a periodic potential and magnetic-field, respectively, drawing connections to twisted MoTe<sub>2</sub>, and (iii) integer filling in toy-models of non-topological flat-bands with a tunable quantum geometry in the presence of repulsive interactions. The partial sum-rule in all of these examples is implicitly constrained by the form of the band quantum geometry via the low-lying excitation spectrum, but is not related to it explicitly. For interacting Slater-determinant insulators, the partial sum-rule is related to a new quantity — “many-body projected quantum geometry” — obtained from the interaction-renormalized electronic bands. We also point out an intriguing connection between the partial sum-rule and the quantum Fisher information associated with the projected many-body position operator. Finding new experimental routes that enable a direct measurement of the quantum geometry in correlated insulators remains an exciting and uncharted territory.

## Contents

		C. Projected quantum weight for interacting Slater determinant states	15
I. Introduction	1	D. Emergent guiding center coordinate in LLL under periodic magnetic field	16
II. “Projected” sum-rule	3		
III. Correlated insulators at partial band-filling	4		
A. Magic-angle twisted bilayer graphene	4		
B. Fractional Chern insulators	6		
1. Lowest Landau-level in a periodic potential	6		
2. Lowest Landau-level in a periodic magnetic field	7		
C. Correlated charge-density wave insulator in trivial flat-bands	9		
IV. Outlook	10		
References	11		
A. Lehmann representation for optical sum-rules	14		
B. Details of Hartree-Fock calculations for MATBG	14		

## I. Introduction

Electronic solids can display insulating behavior due to a variety of non-trivial quantum mechanical reasons, that range from robust band-filling constraints, strong interactions at commensurate lattice fillings, large disorder, and a non-trivial band-topology. Regardless of the underlying mechanism, a universal feature shared by all insulators is their vanishing longitudinal conductivity at zero temperature in the limit of a vanishing frequency (i.e. the Drude weight) [1, 2]:

$$\text{Re}[\sigma_{xx}(\omega \rightarrow 0)] = 0, \quad \text{at } T = 0. \quad (1)$$

In generic quantum many-body systems, computing the detailed frequency dependence of  $\text{Re}[\sigma_{xx}(\omega)]$  can be a priori a non-trivial task. However, in an electrical insulator with a set of fully filled valence bands, the ultraviolet (UV) dynamical response extending out to  $\omega \rightarrow \infty$  satisfies an elegant sum-rule:

$$\mathbb{O} \equiv \int_0^\infty d\omega \frac{\delta_{\mu\nu} \text{Re}[\sigma_{\mu\nu}^L(\omega)]}{\omega} = \frac{\pi e^2}{\hbar} \delta_{\mu\nu} \text{Tr}[g_{\mu\nu}], \quad (2)$$

where  $L$  denotes the longitudinal response, respectively. This is the classic result by Souza-Wilkens-Martin

<sup>\*</sup> Current address: Department of Physics, University of Zürich, 8057 Zürich, Switzerland

<sup>†</sup> Current address: Department of Physics, Princeton University, Princeton, New Jersey 08544, USA

<sup>‡</sup> debanjanchowdhury@cornell.edu

(SWM) [3], described in terms of the trace over the occupied valence states and their quantum geometry,  $g_{\mu\nu}$ , respectively. Quantum geometry [4], while being an old concept [5], has found a resurgence in the field especially with the advent of moiré materials [6]. Specifically, it is now well established that quantum geometry and the so called “ideal-droplet” condition plays an important role in stabilizing Laughlin-like states at fractional fillings of Chern bands [7–9]. In terms of establishing a theoretical connection to experiments, a number of works have investigated the relationship between the quantum geometric properties of the electronic Bloch wavefunctions and their (non-)linear optical response [10–22]. Connections between quantum geometry and entanglement have also been pointed out via different means [23–26].

Various complementary aspects associated with the above sum-rule, including its relationship to polarization fluctuations in insulators have been analyzed previously [27, 28]; an earlier version of a related sum-rule also appeared in Ref. [29]. Recent works have used the above bounds in combination with the analogous  $f$ -sum-rule to put bounds on the insulating gaps and related quantities [30–32], and also highlighted a complementary interpretation of these sum-rules in the time-domain [33, 34]. The above integrated dynamical response is related to a specific coefficient associated with the long-wavelength ( $\mathbf{q} \rightarrow 0$ ) limit of the static momentum-dependent density structure-factor,  $\mathcal{S}(\mathbf{q}) = Kq^2 + \dots$ , where

$$\mathbb{O} = \frac{e^2}{2\hbar} K, \quad (3)$$

and  $K$  is denoted the “quantum weight” [35]. Charge continuity associated with the globally conserved  $U(1)$  density and the insulating property of the ground-state ensures the relationship in Eq. 3.

The UV sum-rule in Eq. 2 extends out to  $\omega \rightarrow \infty$ , and includes all interband transitions (red arrows in Fig. 1). From an experimental point of view, it is impossible to obtain the weight in  $\mathbb{O}$  directly without further assumptions about the high-frequency tails of  $\text{Re}[\sigma^L(\omega)]$ , and (possibly) uncontrolled extrapolations. From a purely theoretical perspective of modeling *correlated* electronic solids, it is rare to have a description that accurately captures the low-energy physics of interest, as well as the high-energy UV degrees of freedom extending out to infinity. Instead, given an interacting effective theory,  $\mathcal{H}_{\text{eff}}(\Lambda)$ , below some physically motivated cutoff,  $\Lambda$ , we are often interested in the low-energy response associated with its ground-state and low-lying excited states. For instance, in the context of magic-angle twisted bilayer graphene (MATBG) [36], the relevant effective theory is typically described in terms of the interactions projected to only a subset of the low-energy bands (Fig. 1). Since the quantum metric controls the minimal spread of the maximally localizable Wannier wavefunctions [37], it is natural to ask the extent to which  $\mathbb{O}$  is related to the notion of a possibly interaction-renormalized quantum geometry tied to  $\mathcal{H}_{\text{eff}}(\Lambda)$ . Our goal here will be

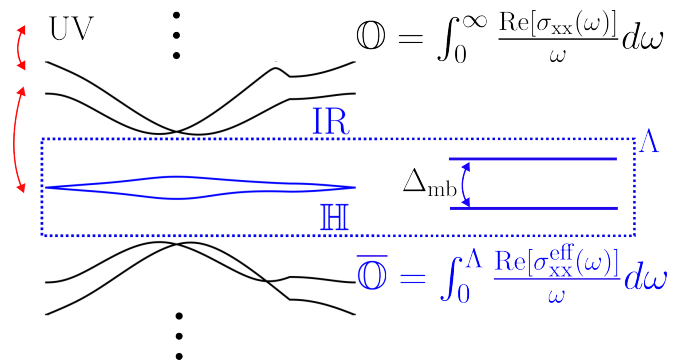


FIG. 1. The non-interacting continuum model dispersion of magic-angle twisted bilayer graphene (MATBG) near  $\theta = 1.08^\circ$ . The UV sum-rule,  $\mathbb{O}$  in Eq. 2 includes all of the inter-band transitions (red arrows). The low energy sum-rule,  $\bar{\mathbb{O}}$  in Eq. 4 only includes the transitions within the projected Hilbert space,  $\mathbb{H}$ , restricted to the energy window  $< \Lambda$  (marked in blue). We will compute  $\mathbb{O}$  for correlation induced insulators at integer filling in MATBG, in solvable models of fractional Chern insulators, and in various insulating states associated with a trivial flat-band but tunable quantum metric.

to analyze the optical absorption spectral weight associated with only the IR transitions (blue arrows in Fig. 1) in solvable, strongly correlated examples of many-body insulators in the isolated “flat-band” setting, and make connections to the underlying quantum geometry.

The remainder of this manuscript is organized as follows: In Sec. II we introduce the central quantity of interest, the projected sum-rule, from a variety of complementary perspectives. In Sec. III we discuss results for the projected optical absorption sum-rule for distinct examples of interaction-induced insulators in (non-)topological flat-band problems. Specifically, in Sec. III A, starting from the chiral flat-band limit of magic-angle twisted bilayer graphene with projected Coulomb interactions, where the spectral weight vanishes, we discuss the effects of a heterostrain-induced band renormalization on the sum-rule. We place these results in the context of the interaction-renormalized quantum geometry of the isolated bands. In Sec. III B, we turn to an evaluation of the projected sum-rule in generalized Laughlin-like states obtained at partial fillings of Landau-level in a periodic field or periodic magnetic-field, respectively, and comment on their relationship to the fluctuations in quantum geometry. We make direct connection to the fractional quantum anomalous Hall states in minimal models of twisted  $\text{MoTe}_2$ . Finally in Sec. III C, we turn to the evaluation of the low-energy sum-rule in trivial symmetry-broken many-body insulating states obtained in topologically trivial flat-bands with a tunable quantum metric. We end with an outlook towards other future directions in Sec. IV. The appendices include a number of technical details.

## II. “Projected” sum-rule

This manuscript will be concerned with *only* the “low-energy” contribution to the optical spectral weight, associated with many-body insulating phases that satisfy Eq. 1. Consider for instance the schematic Fig. 1, where the focus is on the low-energy subspace denoted  $\mathbb{H}$  (shown in blue), that is separated from the high-energy (“remote”) subspace by a bandgap. The effective theory defined in  $\mathbb{H}$  drives the interaction-induced insulating phase, with the fermi-energy ( $\varepsilon_F$ ) placed in the many-body gap ( $\Delta_{\text{mb}}$ ). Let us consider the optical absorption spectral weight in the *projected* subspace ( $\in \mathbb{H}$ ),

$$\overline{\mathbb{O}} \equiv \int_0^\Lambda \mathcal{I}(\omega) d\omega, \text{ where } \mathcal{I}(\omega) = \frac{\text{Re}[\sigma_{\text{xx}}^{\text{eff}}(\omega)]}{\omega}, \quad (4)$$

where  $\Lambda$  is the UV cutoff associated with  $\mathbb{H}$  and  $\sigma_{\text{xx}}^{\text{eff}}$  represents the longitudinal conductivity obtained from  $\mathcal{H}_{\text{eff}}$ . Our modified sum-rule of interest includes all of the inter-band transitions within this low-energy subspace, but not to the high-energy subspace. The central question addressed in this manuscript can also be rephrased differently as follows: *What fraction of the total absorption spectral weight,  $\mathbb{O}$ , is contained in the low-energy theory,  $\mathcal{H}_{\text{eff}}(\Lambda)$ , below an energy scale,  $\Lambda$ ?*

Given that  $\mathbb{O}$  is dominated by an integrand that is large at small  $\omega$ , one might expect the absorption spectral weight is dominated by the low-energy contribution, with most of it contained in  $\overline{\mathbb{O}}$ . It is with this perspective that we revisit the many-body sum-rule for generic insulating ground-states of  $\mathcal{H}_{\text{eff}}$ , restricted to an energy window up to the scale  $\Lambda$ . In this manuscript, we will examine and comment on the low-energy optical absorption spectral weight for a wide class of correlated insulators: (i) flavor symmetry-broken insulators in MATBG at and away from the chiral flat-band limit at integer fillings, (ii) fractional Chern insulators (FCI) due to Coulomb interactions projected to a set of topological vortexable bands inspired by the recent observation of such states in twisted  $\text{MoTe}_2$ , and (iii) an interaction-induced charge-density wave insulator in topologically trivial flat-bands with a tunable quantum metric.

As a result of the projection to the low-energy subspace, it is important to realize that  $\sigma_{\text{xx}}^{\text{eff}}$  is not necessarily due only to a “free-fermion” current. Instead it can include many-body contributions, as is the case for models projected to Landau-levels (LL) or low-energy isolated bands of moiré materials, which we discuss below. We will focus only on many-body phases of matter that satisfy Eq. 1 for the effective conductivity. In the Lehmann representation with a many-body energy eigenbasis  $\{E_n, |n\rangle\}$ , we can rewrite (see Appendix A)

$$\overline{\mathbb{O}} = \pi e^2 \sum_{m,n \in \mathbb{H}} (p_n - p_m) |\langle n | \hat{X} | m \rangle|^2 \theta(E_m - E_n), \quad (5)$$

where  $p_n = e^{-\beta E_n}/Z$ , with  $Z$  the partition function, and  $\hat{X} = \mathbb{P} \hat{X} \mathbb{P}$  is the projected many-body position operator

( $\mathbb{P}$  is the many-body projector to  $\mathbb{H}$ ). The many-body eigenstates are denoted  $|m\rangle \equiv |\Psi_m\rangle$ , with  $m = 0$  labeling the ground-state. At zero temperature, the above simplifies,

$$\overline{\mathbb{O}} \Big|_{T=0} = \pi e^2 \sum_{m \in \mathbb{H}, m \neq 0} |\langle \Psi_m | \hat{X} | \Psi_0 \rangle|^2 \quad (6a)$$

where  $\hat{\rho}_G \equiv |\Psi_0\rangle\langle\Psi_0|$  is the density-matrix (projector) associated with the ground-state wavefunction. When  $\Lambda \rightarrow \infty$ , these reduce to the SWM result in Eq. 2.

The projected theory defined in  $\mathbb{H}$  has an associated *emergent*  $U(1)$  conserved density. Therefore, the arguments leading up to Eq. 3 can be extended to relate the partial optical absorption spectral weight to the structure-factor associated with the projected density,

$$\overline{\mathbb{O}} = \frac{e^2}{2\hbar} \lim_{q \rightarrow 0} \frac{\overline{\mathcal{S}}(\mathbf{q})}{q^2} (\equiv \overline{K}), \quad (7a)$$

$$\text{where } \overline{\mathcal{S}}(\mathbf{q}) \equiv \frac{1}{N} \langle \bar{\rho}_{\mathbf{q}} | \bar{\rho}_{-\mathbf{q}} \rangle - \frac{1}{N} \langle \bar{\rho}_{\mathbf{q}} \rangle \langle \bar{\rho}_{-\mathbf{q}} \rangle, \quad (7b)$$

$$\bar{\rho}_{\mathbf{q}} = \sum_{\alpha, \beta \in \mathbb{H}} \lambda_{\alpha\beta}(\mathbf{k}, \mathbf{q}) c_{\mathbf{k}, \alpha}^\dagger c_{\mathbf{k}-\mathbf{q}, \beta}, \quad (7c)$$

with  $\lambda_{\alpha\beta}(\mathbf{k}, \mathbf{q}) = \langle u_{\mathbf{k}, \alpha} | u_{\mathbf{k}-\mathbf{q}, \beta} \rangle$  is the form factor of the Bloch-states associated with the bands in the projected subspace and  $\alpha, \beta$  denote generic indices including band, orbital and spin, respectively. The quantity  $\overline{K}$  is now the “projected” quantum weight. All of the expectation values  $\langle \dots \rangle$  in Eq. 5 and 7a are meant to be evaluated with respect to the density matrix associated with the many-body insulating state.

While we will mostly focus on results at  $T = 0$  below, it is interesting to also directly evaluate  $\overline{\mathbb{O}}$  in a “high” temperature limit in the same projected subspace, where  $T$  is the largest energy scale in the problem (but implicitly smaller than the bandgap to remote bands). At the leading order in a small- $\beta$ ,

$$\overline{\mathbb{O}}(\beta \rightarrow 0) = \frac{\pi e^2 \beta}{\mathcal{D}_{\mathbb{H}}} \sum_{m,n \in \mathbb{H}} (E_m - E_n) |\langle n | \hat{X} | m \rangle|^2 \theta(E_m - E_n), \quad (8)$$

where  $\mathcal{D}_{\mathbb{H}}$  represents the Hilbert-space dimension. Note that in this high-temperature limit the notion of an “insulating-like” response becomes irrelevant, but we will nevertheless be able to make some rigorous remarks for specific many-body problems. At finite temperature, we can also consider a modified absorption spectral weight,

$$\widetilde{\overline{\mathbb{O}}} = \int_0^\Lambda \mathcal{I}(\omega) \tanh\left(\frac{\omega}{2T}\right) d\omega, \quad (9a)$$

$$= \frac{\pi e^2}{2} \sum_{m,n \in \mathbb{H}} \frac{(p_n - p_m)^2}{p_n + p_m} |\langle n | \hat{X} | m \rangle|^2. \quad (9b)$$

Note that as  $T \rightarrow 0$ ,  $\widetilde{\overline{\mathbb{O}}} \rightarrow \overline{\mathbb{O}}$ , implying no fundamental distinction between the two quantities. Interestingly,  $\widetilde{\overline{\mathbb{O}}}$

represents the quantum Fisher information (QFI) associated with the operator  $\hat{X}$ . The QFI is a well-known object in quantum metrology with connections to entanglement [38–40], and in the above context helps distinguish between the density matrix  $\hat{\rho}$  and its unitarily transformed version,  $\hat{\rho}(\theta) = e^{-i\theta\hat{X}}\hat{\rho}e^{i\theta\hat{X}}$ ; note that  $\hat{\rho}(\theta)$  is effectively the density matrix associated with a “projected” gauge-transformation. We return to this quantity in the outlook, after working our way through all of the examples in the next section.

### III. Correlated insulators at partial band-filling

In the following subsections, we will evaluate the partial sum-rule associated with a variety of correlated insulators inspired by the physics of moiré materials, that range from the spin and/or valley polarized generalized ferromagnets in twisted bilayer graphene, fractional Chern insulators in partially filled Chern bands, and charge-density wave insulators appearing in topologically trivial flat-bands with a tunable quantum metric.

#### A. Magic-angle twisted bilayer graphene

MATBG is a fascinating experimental platform for studying the phenomenology of correlated electrons in a topological nearly flat-band, which has revealed an interesting interplay of correlated insulators and superconductors across its phase-diagram [41–76]. The isolated bands can accommodate 8 electrons per unit cell, usually denoted  $\nu \in [-4, 4]$  on either side of charge neutrality. At all integer fillings, there is an increased tendency to form interaction-induced insulators. The insulating states at  $\nu = \pm 2$  are robust and omnipresent, and with doping they show the most pronounced tendency towards superconductivity. Theoretically, ignoring the bare single-particle dispersion, in the “chiral” limit [77], the strongly-coupled interacting problem effectively maps to the quantum Hall ferromagnet with an enlarged Hilbert space [78, 79]. The continuum effective Hamiltonian for the isolated bands in momentum-space with  $\Lambda$  placed in the bandgap to the remote bands is given by (Fig. 1),  $H_{\text{TBG}} = H_{\text{kin}} + H_{\text{int}}$ , where  $H_{\text{int}} = \frac{1}{2A} \sum_{\mathbf{q}} V_{\mathbf{q}} \bar{\rho}(\mathbf{q})\bar{\rho}(-\mathbf{q})$  and  $\bar{\rho}(\mathbf{q}) = \sum_{\mathbf{k}} \lambda_{\mu}^{\alpha\beta}(\mathbf{k}, \mathbf{q}) c_{\mathbf{k}, \alpha, \mu}^{\dagger} c_{\mathbf{k}-\mathbf{q}, \beta, \mu}$  is the projected density operator. Here  $\lambda_{\mu}^{\alpha\beta}(\mathbf{k}, \mathbf{q}) = \langle u_{\mathbf{k}, \alpha, \mu} | u_{\mathbf{k}-\mathbf{q}, \beta, \mu} \rangle$  is the form-factor constructed out of the Bloch functions, and  $\mu$  denote the valley/spin quantum numbers while  $\alpha, \beta$  denote the sub-lattice indices, and  $A$  represents the area. We consider the double-gated Coulomb interaction given by  $V_{\mathbf{q}} = V_0 d \tanh(qd)/q$ , with  $V_0 = e^2/2\epsilon\epsilon_0 d$ . For later computations, we will take the dielectric constant  $\epsilon = 10$  and the screening length  $d = 25$  nm, with  $V_0 = 18.1$  meV. A standard starting point for  $H_{\text{kin}}$  is the Bistritzer-MacDonald (BM) model [36].

In the chiral-flat band limit,  $H_{\text{TBG}}$  has an exact  $U(4) \times U(4)$  symmetry, leading to a large manifold of degenerate ground states at all integer fillings. Interestingly, the emergent symmetry transformation leaves  $\hat{X}$  invariant, yielding an emergent “dipole” conservation law and a *vanishing*  $\bar{\mathbb{O}} = 0$ , in spite of a non-trivial quantum geometry associated with the renormalized (gapped) electronic bands in the insulating state. To see this, note that in the sub-lattice basis of TBG, we have  $\hat{X} = \sum_{\mathbf{k}} c_{\mathbf{k}, \alpha, \mu}^{\dagger} (i\delta_{\alpha, \alpha'} \partial_{\mathbf{k}_x} + \mathcal{A}_{\mathbf{k}, \alpha\alpha', \mu}) c_{\mathbf{k}, \alpha', \mu}$ ,  $\mathcal{A}_{\mathbf{k}, \alpha\alpha', \mu}^{\nu} = i \langle u_{\mathbf{k}, \alpha, \mu} | \partial_{k_{\nu}} u_{\mathbf{k}, \alpha', \mu} \rangle$  the multi-orbital Berry connection for valley  $\mu$ . Using a gauge-fixing scheme [78] with no non-abelian Berry connection between the two sub-lattices, and the combination of  $C_{2z}$  and particle-hole symmetry (with  $\mathcal{A}_{\mathbf{k}, 1, 1} = \mathcal{A}_{\mathbf{k}}$ ),

$$\hat{X} = \sum_{\mathbf{k}} \hat{c}_{\mathbf{k}}^{\dagger} (i\partial_{\mathbf{k}_x} \mathbf{1} + \mathcal{A}_{\mathbf{k}}^x \sigma_z \tau_z) \hat{c}_{\mathbf{k}}, \quad (10)$$

where  $\sigma$  and  $\tau$  act on the sub-lattice and valley basis, respectively. The ground-state projector commutes with  $\hat{X}$ , leading to the absence of any low-energy optical absorption spectral weight. Note that unlike the LL case, where the vanishing  $\bar{X}$  is tied to the low-energy effective Hamiltonian, in MATBG it is a property only of the ground-state manifold in the chiral flat-band limit. Staying within this manifold, a perturbative correction due to the bare bandwidth  $H_{\text{kin}} \sim O(t)$ , leads to  $\bar{\mathbb{O}} \sim O[(t/V)^2]$ .

To quantify these corrections to  $\bar{\mathbb{O}}$ , we perform self-consistent Hartree-Fock calculations on the continuum model including realistic perturbations away from the chiral-flat band limit to approximate the robust insulating ground-states at filling  $\nu = -2$  (Appendix B); the computations can be straightforwardly generalized to other integer fillings. Deviations from the chiral flat-band limit tend to pick intervalley coherent states, with the precise state being largely determined in experiments by the extrinsic effects of heterostrain ( $\varepsilon$ ). The introduction of small amounts of strain at the graphene scale is enhanced by the moiré pattern, and significantly increase the single-particle bandwidth in addition to breaking various point-group symmetries. To investigate the optical absorption, we calculate  $\bar{\mathbb{O}}$  by exploiting its connection to the low- $q$  behavior of  $\bar{\mathcal{S}}(\mathbf{q})$  as a function of  $\varepsilon$ ; this is shown in Fig. 2(a). At small  $\varepsilon$ , the ground-state is a spin-polarized Kramers-intervalley coherent state (KIVC), which is approximately annihilated by the density operator  $\delta\rho_{\mathbf{q}}$  [78], leading to a large suppression of  $\bar{\mathcal{S}}(\mathbf{q})$  and a small optical absorption spectral weight. Thus, in the limit of a small  $\varepsilon$ , the insulating states remain largely optically “dark”. As  $\varepsilon$  is increased, the ground state projector develops a small  $O(t/V)$  component parallel to the order parameter of a  $C_2\mathcal{T}$  and  $U(1)_V$  preserving semi-metal [78]; the state remains gapped overall. This component is off-diagonal in the sublattice basis and thus no longer commutes with

$\bar{X}$  in Eqn. 10, and is then responsible for the enhancement of  $\bar{\mathcal{O}}$ . Above a critical value of strain, the combined effect of Coulomb renormalization of the bands and strain-induced enhancement of the kinetic energy triggers a translation symmetry breaking order; at  $\nu = -2$  this leads to the incommensurate Kekule spiral (IKS) both within Hartree-Fock mean-field and DMRG studies [80, 81]. In our calculation, this occurs for  $\varepsilon \gtrsim 0.1\%$ , where the state is no longer described as part of the manifold of degenerate ground-states of the chiral model, and instead features a non-trivial winding texture of the inter-Chern coherent component of the order parameter [82, 83]. This strong momentum dependence of the order parameter is inherited from the underlying topology of the TBG bands and due to its Chern-coherent component, it anticommutes with  $\bar{X}$  leading to a further enhancement of  $\bar{\mathcal{O}}$ .

It is also possible to bound the optical absorption spectral weight:  $\bar{\mathcal{O}} \leq \bar{\mathcal{S}}/\Delta_{\text{gap}}$ , where  $\bar{\mathcal{S}}$  represents the low-energy ‘‘partial’’  $f$ -sum-rule associated with the same interacting theory defined in  $\mathbb{H}$  (and has been evaluated previously in Ref. [84]),

$$\bar{\mathcal{S}} \equiv \int_0^\Lambda \text{Re}[\sigma_{\text{xx}}^{\text{eff}}(\omega)] d\omega = \frac{\pi}{2} \langle K_{\text{xx}}^{\text{eff}} \rangle, \quad (11a)$$

$$\langle K_{\text{xx}}^{\text{eff}} \rangle = -\frac{e^2}{h} \frac{1}{A} \text{Tr} \left( [\hat{X}, [\hat{X}, \hat{\rho}_G]] \mathcal{H}_{\text{eff}} \right), \quad (11b)$$

and  $\Delta_{\text{gap}}$  represents the many-body gap in the insulating state. Note that in using the bound on  $\bar{\mathcal{O}}$  in terms of  $\bar{\mathcal{S}}$ , we have assumed that the insulator hosts no sub-gap optical response, i.e.  $\text{Re}[\sigma_{\text{xx}}^{\text{eff}}(\omega)] = 0$  for  $\omega \leq \Delta_{\text{gap}}$ . The comparison between  $\bar{\mathcal{O}}$  and this bound is shown in Fig. 2(a). Here, we see that the bound closely tracks the behavior of the projected quantum weight. However, near the transition point at  $\varepsilon \approx 0.1\%$ , the gap on the KIVC side is reduced by the tendency towards the  $C_2\mathcal{T}$  preserving semi-metal, which makes the bound less accurate as the transition is approached from the low  $\varepsilon$  side. In general this bound is expected to be inaccurate near a quantum phase transition where  $\Delta_{\text{gap}} \rightarrow 0$  but  $\bar{\mathcal{S}}$  remains finite; at  $\nu = -2$  the system remains gapped for the range of  $\varepsilon$  studied in Fig. 2.

Let us now turn to the possible connections between  $\bar{\mathcal{O}}$  and a ‘‘geometric’’ quantity constructed out of the Bloch wavefunctions associated with the active bands. We note at the outset that the quantum metric associated with the bare non-interacting bands is clearly irrelevant for the full response,  $\bar{\mathcal{O}}$ . For any insulating Slater determinant state obtained within the Hartree-Fock approximation, we find that  $\bar{\mathcal{O}}$  can simply be obtained by replacing the quantum metric ( $g_{\mu\nu}$ ) in the sum-rule for  $\mathcal{O}$  in Eq. 2 by a ‘‘projected’’ multi-band quantum metric  $G_{\mu\nu}$  (Appendix C),

$$\bar{\mathcal{O}} = \frac{\pi e^2}{h} \delta_{\mu\nu} \sum_{\mathbf{k}} \text{Tr}[G_{\mu\nu}], \quad \text{where} \quad (12a)$$

$$G_{\mu\nu}^{mn}(\mathbf{k}) = \langle \partial_\mu \tilde{u}_{m,\mathbf{k}} | [\mathcal{P}_{\text{IR}}(\mathbf{k}) - \mathcal{P}_{\text{occ}}(\mathbf{k})] | \partial_\nu \tilde{u}_{n,\mathbf{k}} \rangle \quad (12b)$$

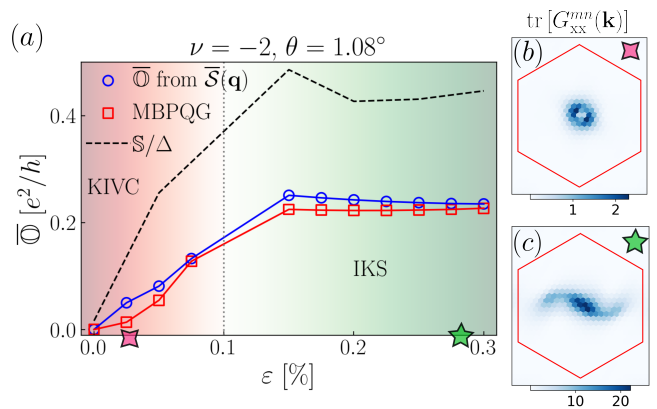


FIG. 2. (a) Projected optical absorption spectral weight,  $\bar{\mathcal{O}}$ , as a function of heterostrain ( $\varepsilon$ ) at  $T = 0$  obtained with respect to the insulating Hartree-Fock ground-state for TBG at  $\nu = -2$  and  $\theta = 1.08^\circ$ . The blue circles correspond to  $\bar{\mathcal{O}}$  extracted by fitting the small- $q$  behavior of  $\bar{\mathcal{S}}(\mathbf{q})$  using Eqn.7b, and the black dashed line corresponds to the upper bound,  $\bar{\mathcal{S}}/\Delta_{\text{gap}}$ . The red squares correspond to  $\bar{\mathcal{O}}$  evaluated using the many-body projected quantum geometry (MBPQG) in Eq. 12a. MBPQG for (b) KIVC order at  $\varepsilon = 0.025\%$ , and (c) IKS order at  $\varepsilon = 0.275\%$  in the  $\mathbf{q}_{\text{IKS}}$  boosted Brillouin zone.

Here, the trace is taken over the occupied Hartree-Fock bands, and  $|\tilde{u}_{n,\mathbf{k}}\rangle$  denotes the Hartree-Fock renormalized Bloch wavefunction. The projectors,

$$\mathcal{P}_{\text{IR}}(\mathbf{k}) = \sum_{m \in \text{IR}} |\tilde{u}_{m,\mathbf{k}}\rangle \langle \tilde{u}_{m,\mathbf{k}}|, \quad (13a)$$

$$\mathcal{P}_{\text{occ}}(\mathbf{k}) = \sum_{m \in \text{occ}} |\tilde{u}_{m,\mathbf{k}}\rangle \langle \tilde{u}_{m,\mathbf{k}}|, \quad (13b)$$

are associated with the (occupied) Hartree-Fock bands in the IR theory. Note that  $G_{\mu\nu}^{mn}(\mathbf{k})$  is different compared to the usual multi-band quantum geometric tensor since  $\mathcal{P}_{\text{IR}}(\mathbf{k})$  is not identity. Relatedly, the integral of  $G_{\mu\nu}^{mm}(\mathbf{k})$  is not related to the minimal spread of any many-body Wannier wavefunction associated with the renormalized bands, since the Slater-insulators in the chiral flat-band limit have a vanishing  $\sum_{\mathbf{k}} \text{Tr}[G_{\mu\nu}]$  even though they are not atomic insulators. We should view  $G_{\mu\nu}^{mn}(\mathbf{k})$  as a new quantity, which we dub ‘‘many-body projected quantum geometry’’ (MBPQG). It is easy to verify that it is positive semi-definite and bounded from above by the band quantum geometry (Appendix C). Hence, we can think of MBPQG as accounting for the low-energy ‘‘active’’ part of the spreading of the Wannier wavefunction. We have evaluated  $\bar{\mathcal{O}}$  using Eq. 12a in Fig. 2(a). To help visualize the MBPQG associated with the interaction-renormalized (filled) bands, we plot  $\delta_{\mu\nu} \text{Tr}[G_{\mu\nu}](\mathbf{k})$  in the continuum model for two different values of  $\varepsilon$  in Fig. 2(b) in the KIVC and IKS phases, respectively.

## B. Fractional Chern insulators

A number of recent experimental breakthroughs have led to the observation of FCI [85–88], or fractional quantum anomalous Hall (FQAH) insulators [89], in moiré transition metal dichalcogenide (TMD) [90–92] and multilayer graphene materials [93]. We address here the fraction of the total spectral weight,  $\mathbb{O}$ , that is contained in  $\overline{\mathbb{O}}$  for these insulating states. Regardless of the microscopic mechanism (which may involve various forms of symmetry-breaking [68, 94–97]), the low-energy physics for many of the FCI/FQAH insulators is described via Coulomb interactions projected to a set of nearly flat and isolated topological (Chern) bands having near-ideal quantum geometry (“vortexability”) [98]; see also effects of interaction-induced band-mixing across the single-particle gap on the stability of FCI [88, 99–102]. We will ignore any band-mixing effects and focus only on the “projected” limit in this manuscript, where many of the recently discovered FCI states can be approximated by a generalized Laughlin-like character [9, 103–106]. The low-energy theory is then described by placing  $\Lambda$  inside the bandgap,  $E_{\text{band}}$ , to the remote bands. A recent work [107] has addressed the question of the low-energy optical absorption in FCI’s numerically for vortexable bands starting from the LLL limit, and argued that the response is “weak”. In what follows, we will be able to shed some complementary analytical insights into what controls the weak response and make connections to the moiré TMD materials; we return to comparisons with this work in Sec. III B 2.

We begin by summarizing the results for a low-energy theory that describes the classic problem of interactions projected to the lowest (spinless) LL;  $\Lambda$  is now a scale that resides in the cyclotron-gap to the first LL. Recall that in the absence of disorder,  $\hat{X}$  is an emergent conserved operator, and thus the many-body energy eigenstates  $|n\rangle \in \mathbb{H}$  can be simultaneously diagonalized in the  $\hat{X}$ -basis. Thus, we immediately infer that  $\overline{\mathbb{O}} = 0$  in this theory. In fact,  $\overline{\mathbb{O}}$  vanishes at *any* filling of the lowest Landau level (LLL), even when the spectrum does *not* have a gap while satisfying Eq. 1 [108]. The latter is a consequence of Kohn’s theorem, stating that the  $f$ -sum-rule is saturated at the cyclotron frequency with  $\text{Re}[\sigma_{xx}(\omega)] = 0$  for  $\omega < \omega_c$  [109, 110]. The vanishing  $\overline{\mathbb{O}}$  in the LLL theory for both quantum Hall insulators and for metallic phases, such as the composite Fermi liquid [111], is consistent with the known results for the projected structure factor in Eq. 7a, which vanishes as  $\overline{\mathcal{S}}(\mathbf{q}) \sim q^4$  in the former [112, 113], and as  $q^3$  in the latter [114, 115], respectively. Interestingly, within this projected theory,  $\overline{\mathbb{O}}(\beta \rightarrow 0)$  in Eq. 8 also vanishes. Therefore, given the structure of the many-body matrix elements of  $\hat{X}$ , in the theory for a partially filled LLL, the entire absorption spectral weight associated with  $\mathbb{O}$  is saturated by  $(\mathbb{O} - \overline{\mathbb{O}})$  at all temperatures. Clearly, the LLL has a non-vanishing (uniform) quantum geometry, which is *irrele-*

*vant* for determining the *low-energy* optical absorption spectral weight. However, as we show below, the *fluctuations* in quantum geometry can control the low-energy spectral weight.

The vanishing low-energy spectral weight in LLL is due to the conservation of center-of-mass (or dipole moment) at low-energy. In general, any term that breaks dipole symmetry contributes to the low-energy spectral weight. Let us first give a generic argument for the strength of this response, and then we will discuss individual cases. By definition,  $\overline{\mathbb{O}}$  is positive semi-definite and it has a lower bound, namely,

$$\overline{\mathbb{O}} \Big|_{T=0} \geq \pi e^2 |\langle \Psi_e | \hat{X} | \Psi_g \rangle|^2 = \pi e^2 \frac{|\langle \Psi_e | [\hat{X}, \mathcal{H}_{\text{eff}}] | \Psi_g \rangle|^2}{\Delta^2}, \quad (14)$$

where  $|\Psi_e\rangle$  is the first excited state and  $\Delta = E_e - E_g$  is the energy gap. If we consider a gapped fractional quantum Hall state obtained by perturbing away from the dipole-conserving limit, this automatically implies that  $\overline{\mathbb{O}} \Big|_{T=0}$  is in general finite. Note that for systems with open boundary condition,  $\Delta$  and  $|\Psi_e\rangle$  should be viewed as bulk gap and bulk excitation, respectively. For systems on a torus,  $\hat{X}$  should be viewed as taking the  $\mathbf{q} \rightarrow 0$  limit in  $\bar{\rho}\mathbf{q}$ . In order to vary  $\mathbf{q}$  continuously, one then needs to perform flux-threading in the torus. Numerical exact-diagonalization studies that target only the low-lying states and the associated structure-factor for relatively large system-sizes can in principle be used to estimate the strength of this low-energy response.

For LLL, two types of dipole symmetry breaking perturbation have been pointed out (not involving disorder [116]): (i) a spatially periodic potential, and (ii) a spatially periodic magnetic field. We consider them individually in the next two subsections.

### 1. Lowest Landau-level in a periodic potential

For a weak periodic potential, the low-energy Hilbert space is still described in terms of the original LLL, and the projected periodic potential can be written as  $H_{\text{pot}} = \sum_{\mathbf{G}} V_{\mathbf{G}} \bar{\rho}_{\mathbf{G}}$ , where  $\mathbf{G}$  is the reciprocal lattice vector associated with the periodic potential and  $V_{\mathbf{G}}$  represents its strength. Using the single mode approximation [112], and a Laughlin-like wavefunction for the ground-state [117], we can approximate

$$\overline{\mathbb{O}} \approx \frac{e^2}{4\hbar} \sum_{\mathbf{G}} l_B^2 |\mathbf{G}|^2 \frac{|V_{\mathbf{G}}|^2}{\Delta_{\mathbf{G}}^2} \overline{\mathcal{S}}_0(\mathbf{G}), \quad (15a)$$

$$\overline{\mathcal{S}} \approx \frac{e^2}{4\hbar} \sum_{\mathbf{G}} l_B^2 |\mathbf{G}|^2 \frac{|V_{\mathbf{G}}|^2}{\Delta_{\mathbf{G}}} \overline{\mathcal{S}}_0(\mathbf{G}), \quad (15b)$$

where  $l_B$  is the magnetic length,  $\Delta_{\mathbf{G}}$  denotes the gap for the collective excitation at  $\mathbf{G}$ , and  $\overline{\mathcal{S}}_0(\mathbf{G})$  is the structure

factor evaluated with respect to the Laughlin state.

## 2. Lowest Landau-level in a periodic magnetic field

Periodic magnetic field in the LLL has been proposed as a theoretical tool to study (fractional) Chern insulating states across moiré systems [9, 98, 103, 104, 106, 107, 118–120]. A uniform magnetic field gives rise to uniform Berry curvature in the magnetic Brillouin zone and the fluctuation of the magnetic field in real space controls the fluctuation of the Berry curvature in momentum space. The LLL in the periodic magnetic field is given by the zero modes of the operator  $(-i\partial - \hat{A})$ , where  $\partial \equiv \partial_x + i\partial_y$  and  $\hat{A} \equiv A_x + iA_y$ ,  $A_\mu$  being the vector potential [121, 122]. Therefore, the wavefunction can be written as  $\psi_{LLL}(\mathbf{r}) = f(z)e^{-\varphi(\mathbf{r})}$ , where  $\partial_\mu^2 \varphi(\mathbf{r}) = B(\mathbf{r})$ . Hence, the projected Hilbert space has a different basis compared to the LLL under uniform magnetic field and the dipole conservation is broken from the projection in  $\mathcal{H}_{\text{eff}}$ . For  $B(\mathbf{r})$  that is periodic in space, there is discrete magnetic translation symmetry, which allows us to define a magnetic Brillouin zone. The relationship between  $B(\mathbf{r})$  and the Berry curvature  $\mathcal{B}_k$  can be obtained from the Bloch wavefunction, but the generic analytical form is cumbersome so we only give an approximate expression. If  $B(\mathbf{r}) \equiv B_0 + B_1(\mathbf{r}) = 1 + \phi_1 \sum_j e^{i\mathbf{k}_j \cdot \mathbf{r}}$ , where  $B_0 = 1$  denotes the uniform part and  $\mathbf{k}_j$  denotes the reciprocal lattice vectors, to the leading order in  $\phi_1$ ,  $\mathcal{B}_k \approx 1 - \phi_1 \sum_j e^{i\mathbf{k}_j \wedge \mathbf{k}} - \frac{|\mathbf{k}_j|^2}{4}$  [123].

We summarize our results of the low-energy spectral weight schematically in Fig. 3a. For the LLL under a uniform magnetic field, Kohn's theorem dictates that the dipole transition is purely inter-LL (Fig. 3b). However, under a periodic magnetic field, the fluctuation of the magnetic field  $\delta B \sim \phi_1$  enables intra-LL dipole transition (Fig. 3d), resulting in a finite  $\bar{\mathcal{O}}$  and  $\bar{\mathcal{S}}$ , proportional to  $(\delta B)^2$  to the leading order.

For a small  $\phi_1$ , the dipole matrix element can be written as,

$$\hat{X} = \hat{X}_0 + \sum_{n=1}^{\infty} (\phi_1)^n \hat{X}_n, \quad (16)$$

where the subscript '0' denotes the matrix of the projected position operator under  $B_0$ , and the subscript 'n' denotes the n-th order correction. Recall that  $[\hat{X}_0, \hat{Y}_0] = -i/B_0$ , which is the so-called "emergent" guiding center [124, 125]. Since the center-of-mass coordinate no longer commutes with the projected Hamiltonian, the ground state can be written as  $|\tilde{\Psi}\rangle = |\Psi^0\rangle + \sum_{n=1}^{\infty} (\phi_1)^n |\Psi^n\rangle$ , where  $|\Psi^0\rangle$  is the eigenstate of  $\hat{X}_0$ .

The leading order contribution in  $\bar{\mathcal{O}} \Big|_{T=0}$  is of order  $\phi_1^2$ , and the coefficient is positive semi-definite by definition. To be explicit,  $\bar{\mathcal{O}} \Big|_{T=0} = \pi e^2 \phi_1^2 \langle \eta | (1 - |\Psi^0\rangle \langle \Psi^0|) | \eta \rangle +$

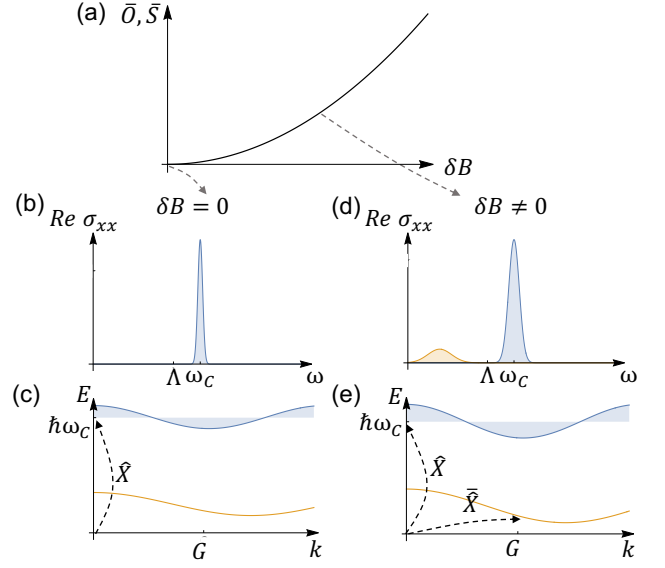


FIG. 3. Schematic summary of the optical sum-rules and allowed transitions in the LLL. (a) For a small fluctuation of the magnetic field,  $\delta B$ , the strength of  $\bar{\mathcal{O}}$  and  $\bar{\mathcal{S}}$  is quadratic in  $\delta B$ . For a uniform [periodic]  $B$ , the optical absorption and the dispersion of the collective modes are sketched in panels (b) [(d)] and (c) [(e)], respectively. The periodic  $B$  can change the energetic of the states of higher LL, resulting in broader optical absorption near  $\omega_c$  [panel (d)]. The breaking of continuous magnetic translation symmetry by the spatial fluctuation  $\delta B$  enables intra-LL optical transition, which excites collective modes at momentum of the reciprocal lattice vector [panel (e)].

$O(\phi^4)$ , where  $|\eta\rangle = \hat{X}_0 |\Psi^1\rangle + \hat{X}_1 |\Psi^0\rangle$ . Although we cannot solve for  $|\Psi^0\rangle$  and  $|\Psi^1\rangle$  exactly, we can make progress in estimating the projected spectral weight by approximating the ground state  $|\tilde{\Psi}\rangle$  at fractional fillings by generalized Laughlin states [9], which amounts to ignoring the contribution from  $|\Psi^n\rangle$  for  $n \geq 1$ .

On the plane, the generalized Laughlin state can be written as  $\Psi_{gL}(\mathbf{x}_1, \dots, \mathbf{x}_N) = R^{-1} \prod_{i < j} (z_i - z_j)^m e^{-\sum_i \varphi(\mathbf{x}_i)}$ , recalling that  $\partial_\mu^2 \varphi(\mathbf{r}) = B(\mathbf{r})$  and therefore  $\varphi(\mathbf{r}) = |z|^2/4 + \tilde{\varphi}(\mathbf{r})$  for  $B(\mathbf{r}) = 1 + \tilde{B}(\mathbf{r})$ . Without the  $\tilde{\varphi}(\mathbf{x}_i)$  term,  $\Psi_{gL}$  is the original Laughlin wavefunction with filling fraction  $\nu = 1/m$ , and  $R$  being the normalization constant. We note that  $|\Psi_{gL}\rangle$  can be viewed as a special  $|\Psi^0\rangle$  that is annihilated by  $\hat{X}_0$  [124]. However, since the generic projected density-density interaction does not conserve the "emergent" guiding center,  $|\Psi_{gL}\rangle$  is not the exact ground state except for some special pseudo-potential Hamiltonian [104]. Nonetheless, we assume  $|\Psi_{gL}\rangle$  is a good approximation to the true ground state, and a direct evaluation of  $\bar{\mathcal{O}}$  with respect to this

state yields,

$$\begin{aligned}\bar{\mathbb{O}}_{gL} &\equiv \pi e^2 \langle \Psi_{gL} | \hat{X} (1 - |\Psi_{gL}\rangle \langle \Psi_{gL}|) \hat{X} | \Psi_{gL} \rangle \\ &= \pi e^2 \phi_1^2 \langle \Psi_{gL}^0 | \hat{X}_1 (1 - |\Psi_{gL}^0\rangle \langle \Psi_{gL}^0|) \hat{X}_1 | \Psi_{gL}^0 \rangle + O(\phi_1^4),\end{aligned}\quad (17)$$

where  $|\Psi_{gL}^0\rangle$  denotes the Laughlin wavefunction under uniform magnetic field. Note that the correction from the periodic part of the magnetic field to the wavefunction only appears at a higher order in  $O(\phi_1^2)$ .

In order to obtain  $\hat{X}_1$  explicitly, we consider the projected density operator under a periodic magnetic field. From the LLL wavefunction, we have [122, 123],

$$\hat{\rho}_{\mathbf{q}} = \hat{\rho}_{\mathbf{q}}^0 + \frac{\phi_1}{|G|^2} \sum_j \hat{\rho}_{\mathbf{q}+\mathbf{k}_j}^0 \left[ 2 - \left( e^{\frac{\bar{k}_{jx}q}{2}} + e^{\frac{k_{jy}q}{2}} \right) \right], \quad (18)$$

where  $q = q_x + iq_y$  and analogously for  $k_j$ , and the superscript ‘0’ denotes the density operators that satisfy GMP algebra [112],

$$[\hat{\rho}_{\mathbf{q}_1}^0, \hat{\rho}_{\mathbf{q}_2}^0] = 2i \sin \frac{\mathbf{q}_1 \wedge \mathbf{q}_2}{2} \hat{\rho}_{\mathbf{q}_1+\mathbf{q}_2}^0, \quad \text{where} \quad (19a)$$

$$\hat{\rho}_{\mathbf{q}}^0 = \hat{\rho}^0 e^{\frac{i\mathbf{q}^2}{4}}, \quad \text{and} \quad \mathbf{q}_1 \wedge \mathbf{q}_2 = \epsilon_{\mu\nu} q_{1,\mu} q_{2,\nu} \quad (19b)$$

In the small  $\mathbf{q}$  limit of  $\hat{\rho}_{\mathbf{q}}$ , we have  $\hat{\rho}_{\mathbf{q}} = i\mathbf{q} \cdot \hat{X}$  (see Appendix D) and

$$\hat{X}_1 = -\frac{i}{|G|^2} \sum_j k_{j,x} \hat{\rho}_{\mathbf{k}_j}^0, \quad (20)$$

which gives

$$\bar{\mathbb{O}}_{gL} = \frac{\pi e^2 \phi_1^2}{|G|^4 l_B^2} \sum_j k_{j,x}^2 \bar{\mathcal{S}}_0(\mathbf{k}_j). \quad (21)$$

Similarly, we can obtain the partial  $f$ -sum-rule,  $\bar{\mathcal{S}}_{gL}$ . Again, the leading order contribution is of order  $\phi_1^2$  and therefore we only need to consider the order  $\phi_1$  term in  $\mathcal{H}_{\text{eff}}$ ,

$$\bar{\mathcal{S}}_{gL} \equiv -\frac{e^2}{4} \langle \Psi_{gL} | \left[ \hat{X}, \left[ \hat{X}, \mathcal{H}_{\text{eff}} \right] \right] | \Psi_{gL} \rangle \quad (22a)$$

$$\begin{aligned}&= -\frac{e^2}{4} \phi_1^2 \langle \Psi_{gL}^0 | \left[ \hat{X}_1, \left[ \hat{X}_1, \mathcal{H}_{\text{eff}}^0 \right] \right] | \Psi_{gL}^0 \rangle \\ &\quad -\frac{e^2}{4} \phi_1^2 \langle \Psi_{gL}^0 | \left[ \hat{X}_1, \left[ \hat{X}_0, \mathcal{H}_{\text{eff}}^1 \right] \right] | \Psi_{gL}^0 \rangle + O(\phi_1^4),\end{aligned}\quad (22b)$$

where  $\mathcal{H}_{\text{eff}} \equiv \sum_{\mathbf{q}} V_{\mathbf{q}} \hat{\rho}_{\mathbf{q}} \hat{\rho}_{-\mathbf{q}} = \mathcal{H}_{\text{eff}}^0 + \phi_1 \mathcal{H}_{\text{eff}}^1 + O(\phi_1^2)$ . From discrete rotation symmetry on a lattice, one finds that the second term in the last line of the above equation vanishes and therefore,

$$\bar{\mathcal{S}}_{gL} = \frac{e^2 \phi_1^2}{4|G|^4 l_B^2} \sum_j k_{j,x}^2 \bar{f}_0(\mathbf{k}_j), \quad (23)$$

where  $\bar{f}_0(\mathbf{k}_j) = \langle \left[ \hat{\rho}_{\mathbf{k}_j}^0, \left[ \hat{\rho}_{-\mathbf{k}_j}^0, \mathcal{H}_{\text{eff}}^0 \right] \right] \rangle$  is the projected oscillator strength [112].

Let us now apply our formalism to the correlated insulators in twisted homobilayer TMD, and address the question of how large is  $\bar{\mathbb{O}}$  (and  $\bar{\mathbb{O}}$ ). First, we would like to comment on the validity of the leading order expansion in  $\phi_1$ . Although  $\phi_1$  quantifies the fluctuation of the magnetic field in space, since the wavefunction involves  $\tilde{\varphi}(\mathbf{x})$ , the expansion parameter is actually  $\phi_1/(|G|^2 l_B^2)$ , which can be parametrically smaller than  $\phi_1$ . For example, for a periodic modulation with  $2\pi$ -flux per unit cell,  $|G|^2 l_B^2 = 2\pi$  for square lattice and  $4\pi/\sqrt{3}$  for triangular lattice. In twisted homobilayer TMD systems, the moiré lattice potential generates an effective magnetic field  $B_{\text{eff}}(\mathbf{r})$  [106]. We keep the first five shells of the reciprocal lattice vector and write,

$$B_{\text{eff}}(\mathbf{r}) = 1 + \sum_{n=1}^5 \sum_j \phi_{n,j} e^{i\mathbf{k}_{n,j} \cdot \mathbf{r}}, \quad (24)$$

where  $n$  labels the shell and  $j$  labels the different reciprocal lattice vectors within one shell of the same  $|\mathbf{k}_{n,j}|$ . From the first-order expansion, the Berry curvature can be written as  $B_{\text{eff}}(\mathbf{k}) = 1 - \sum_{n=1}^5 \sum_j \phi_{n,j} e^{i\mathbf{k}_{n,j} \wedge \mathbf{k} - \frac{|\mathbf{k}_{n,j}|^2}{4}}$ . We compare  $B_{\text{eff}}(\mathbf{k})$  with the Berry curvature obtained from the continuum model of the same system in Fig. 4 and observe that the first-order approximation already provides qualitative agreement with the continuum model.

In order to compute  $\bar{\mathbb{O}}_{gL}$ ,  $\bar{\mathcal{S}}_{gL}$  in Eq. 21 and 23, we need the numerical values of  $\bar{\mathcal{S}}_0(\mathbf{k}_j)$  and  $\bar{f}_0(\mathbf{k}_j)$ . These can be obtained from the known Monte-Carlo results for  $\bar{\mathcal{S}}_0(\mathbf{q})$ , and the relationship between  $\bar{\mathcal{S}}_0(\mathbf{q})$  and  $\bar{f}_0(\mathbf{q})$  for the Laughlin state at  $\nu = 1/3$  [112]. Here we use the 1/3 generalized Laughlin state to estimate the intra-band transition of the fractional Chern insulator at filling fraction  $-2/3$  of the twisted bilayer TMD systems [90, 91]. Counting the electron filling,  $\nu = -2/3$  corresponds to a fully filled valence band for one valley, which is inert given that valley d.o.f. is a good quantum number, and a 1/3 filled valence band for the other valley.

To take into account multiple momentum shells, we replace  $\frac{k_{j,x}^2}{|G|^4}$  by  $\frac{k_{n,j,x}^2}{|\mathbf{k}_{n,j}|^4}$ , and obtain  $\bar{\mathbb{O}}_{gL} \approx 2.73 \times 10^{-4} e^2/\hbar$  and  $\bar{\mathcal{S}}_{gL} \approx 2.76 \times 10^{-5} (e^2/\epsilon l_B)$ , where the interaction is taken to be Coulomb,  $V(r) = e^2/\epsilon r$ , with  $\epsilon$  being the dielectric constant. Here we ignore the contribution from the gate screening since  $|\mathbf{k}_1|d \gg 1$  for the first momentum shell and a typical gate distance  $300 \text{ \AA}$  [90]. Interestingly, both of these optical spectral weights are numerically ‘‘small’’ in the relevant units for a weak ( $\delta B$ ), suggesting that most of the absorption would be associated with excitations to the remote degrees of freedom, contained in  $\mathbb{O} - \bar{\mathbb{O}}$ . This is in line with previous complementary analysis that highlighted the ‘‘dark’’ nature of the FCI states in the moiré setting [107].

The strength of the effective magnetic field does not depend on the twist angle except for an overall scaling



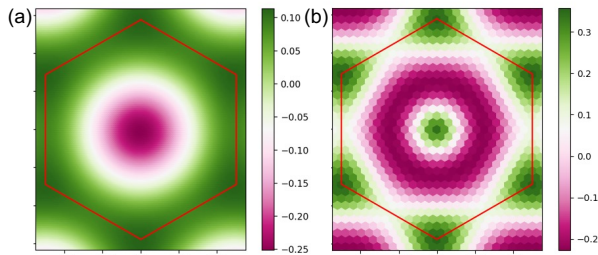


FIG. 4. Berry curvature fluctuation calculated using the (a) effective magnetic field in Eq. 24, and (b) continuum model for twisted homobilayer MoTe<sub>2</sub>. The red hexagon marks the Brillouin zone, where the background uniform Berry curvature is normalized to 1. The effective magnetic field is obtained from the unitary transformation formalism in Ref. [106] using the same parameters as the continuum model for unstrained MoTe<sub>2</sub> at twist angle 1.5° [126]. For the effective magnetic field, we retain the first five Fourier components (excluding the zero momenta) to be -0.251, -0.316, 0.478, -0.138, 0.0804.

factor that does not affect  $\overline{\mathbb{O}}_{gL}$  and  $\overline{\mathbb{S}}_{gL}$ . However, the twist angle controls the deviation of the periodic LLL limit [107]. As long as the FCI state still persists, the leading order perturbation can be viewed as a periodic potential applied to LLL and the discussion in the previous section follows. To give an estimate of the magnitude, the strength of the periodic potential  $V_{\mathbf{G}}$  is of the same order as the band-width, which depends on the deviation of the twist angle  $\theta$  from the angle where the bare bandwidth is minimized. The gap  $\Delta_{\mathbf{G}} \approx 0.2(e^2/\epsilon l_B)$  from SMA. For  $\theta = 3.7^\circ$  and dielectric constant  $\epsilon = 8$  [90],  $\Delta_{\mathbf{G}} \approx 6.6$  meV. Hence for a bandwidth  $\sim 10$  meV,  $V_{\mathbf{G}}/\Delta_{\mathbf{G}} \sim O(1)$ . Therefore, the dispersion induced by twist angle contributes to  $\overline{\mathbb{O}} \sim \overline{\mathbb{S}}_0(\mathbf{G})e^2/\hbar = 0.021e^2/\hbar$  and  $\overline{\mathbb{S}} \sim V_{\mathbf{G}}\overline{\mathbb{S}}_0(\mathbf{G}) \sim 0.21$  meV. The reduction of the spectral weight from the “bare” bandwidth comes from the smallness of the projected structure factor  $\overline{\mathbb{S}}_0(\mathbf{G})$ .

### C. Correlated charge-density wave insulator in trivial flat-bands

Let us now turn our attention to topologically trivial flat-bands which display intertwined phases driven by interaction effects near commensurate fillings. In this regard, one of us has recently analyzed a model of spinful electrons ( $s = \uparrow, \downarrow$ ) with two orbitals ( $\ell = 1, 2$ ) on a square lattice (with spacing,  $a$ , set to unity) using non-perturbative quantum Monte-Carlo (QMC) computations [127]. The Hamiltonian is given by,  $H = H_K + H_I$ ,

where

$$H_K = -t \sum_{\mathbf{k}} \hat{\mathbf{c}}_{\mathbf{k}}^\dagger (\tau_x \sin \alpha_{\mathbf{k}} + \sigma_z \tau_y \cos \alpha_{\mathbf{k}} + \mu \tau_0) \hat{\mathbf{c}}_{\mathbf{k}}, \quad (25a)$$

$$\alpha_{\mathbf{k}} = \zeta (\cos k_x + \cos k_y),$$

$$H_I = -\frac{U}{2} \sum_{\mathbf{r}, \ell} \delta \hat{n}_{\mathbf{r}, \ell}^2 + V \sum_{\langle \mathbf{r}, \mathbf{r}' \rangle, \ell} \delta \hat{n}_{\mathbf{r}, \ell} \delta \hat{n}_{\mathbf{r}', \ell}. \quad (25b)$$

We have combined the electronic operators into the vector,  $\hat{\mathbf{c}}_{\mathbf{k}}^\dagger$ , with the Pauli-matrices  $\hat{\sigma}$  and  $\hat{\tau}$  acting on the spin and orbital indices, respectively. Note that  $H_K$  hosts two completely flat bands with energies,  $\epsilon_{\mathbf{k}} = \pm t$ , regardless of the parameter,  $\zeta$ . The latter controls the minimal spatial extent of the localized Wannier functions with an integrated quantum metric,  $\zeta^2/2$ . The local interaction terms acting on the shifted density operator,  $\delta \hat{n}_{\mathbf{r}, \ell} = \sum_s \hat{c}_{\mathbf{r}, \ell, s}^\dagger \hat{c}_{\mathbf{r}, \ell, s} - 1$ , include an attraction,  $U$ , and nearest-neighbor repulsion,  $V$ , which controls the competition between distinct many-body ground-states. In the non-interacting limit at a finite filling ( $\nu$ ), the only insulating phases are band-insulators at  $\nu = 2$  associated with a fully filled  $\epsilon_{\mathbf{k}} = -t$  band with the chemical potential inside the bandgap. Including all of the inter-band transitions between the filled and empty states ( $\epsilon_{\mathbf{k}} = t$  band) leads to,

$$\mathbb{O} = 2 \frac{\pi e^2}{\hbar} \sum_{\mathbf{k}} (\partial_x \alpha_{\mathbf{k}})^2 = \frac{\pi e^2 \zeta^2}{\hbar}, \quad (26)$$

in line with the expectations of the standard SWM result in this simplified setting of just two bands (each of which is two-fold spin degenerate). Clearly in the same band-insulating state a weak  $U$ ,  $V$  (compared to the bandgap) does not affect the result.

Using QMC, we have previously obtained the numerically exact many-body phase-diagram in the “projected” limit where  $\{V, U\} \lesssim E_{\text{gap}} (= 2t)$  for the entire range of filling of the lower flat-band ( $\epsilon_{\mathbf{k}} = -t$ ), as a function of  $\zeta$  and different ratios of  $V/U$ . Notably, for a finite  $\zeta$  and  $V = 0$ , and for  $U/t = 1$  the ground state is a superconductor at all fillings  $0 < \nu < 2$ . However, for  $V \ll U$  and half-filling of the lower band ( $\nu = 1$ ), the ground-state is a charge-density wave (CDW) insulator of pre-formed Cooper-pairs. We are thus interested in  $\overline{\mathbb{O}}$  for the insulating state when  $\Lambda$  lies inside the bandgap to the remote bands, i.e. the remote bands are projected out (Fig. 5). Note that for a finite doping,  $\delta\nu$ , away from this commensurate filling the ground-state is a “supersolid” (SS), which implies that  $\overline{\mathbb{O}}$  diverges with  $\delta\nu = |\nu - 1|$ .

Firstly, in the limit of  $\zeta \rightarrow 0$ , which is effectively a decoupled “classical” limit,  $\overline{\mathbb{O}} \rightarrow 0$  vanishes trivially; a chiral symmetry forbids an  $O(\zeta)$  contribution. Second, since the CDW-insulator at  $\nu = 1$  melts and yields a superconductor for  $V \rightarrow 0$ , we expect  $\overline{\mathbb{O}}$  to diverge in this limit. Finally, the QMC also found a continuous quantum phase transition from a CDW insulator to a SS

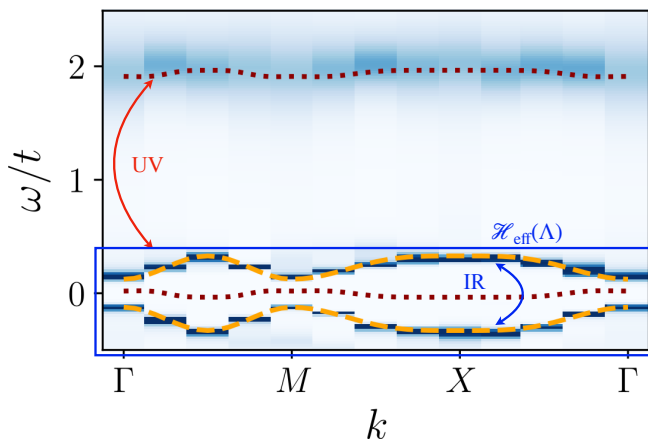


FIG. 5. The gapped single-electron spectral functions for the model in Eq. 25b obtained via (analytically continued) QMC computations in the CDW phase at  $\nu = 1$  (see Ref. [127] for details). The microscopic parameters are  $U/t = 1$ ,  $V/t = 0.08$ . Red dotted lines denote the original flat bands while the dashed orange lines represent the interaction-renormalized bands. In the band-insulator at  $\nu = 2$ , the UV interband transitions determine  $\mathbb{O}$  as in Eq. 26. In the effective theory,  $\mathcal{H}_{\text{eff}}$ , the inter-band transitions within the low-energy subspace controls  $\overline{\mathbb{O}}$  (Eq. 27).

across a critical  $\zeta_c$  at a fixed  $V$  and filling  $\nu = 1$ . This transition must also be accompanied by a diverging  $\overline{\mathbb{O}}$ . Combining all of these constraints at a fixed  $\nu = 1$ , we expect,

$$\overline{\mathbb{O}} = \zeta^2 |\zeta_c - \zeta|^{-|\alpha|} \mathcal{G}_\zeta \left( \frac{V}{U} \right), \quad (27)$$

where  $\mathcal{G}_\zeta(x \rightarrow 0) \rightarrow \infty$  exhibits a smooth dependence on  $\zeta$ , and  $|\alpha|$  is a universal critical exponent. Notably, once again, we observe a complex low-energy absorption spectral weight that is not simply related to the bare quantum metric,  $\zeta$ . Moreover, given that the CDW to SS transition does not exhibit any single-particle gap-closing (Fig. 5), or any singular features in the single-particle response, the above quantity can not be interpreted simply as the quantum geometry of the interaction-renormalized bands either (Fig. 5).

#### IV. Outlook

Electronic insulators that arise due to strong interaction-induced effects at a partial band-filling represent one of the most fascinating quantum phases of matter. Their low-energy optical absorption encodes useful information about the many-body spectrum and the nature of dipole transitions between the filled and empty states, respectively. In this manuscript, we have analyzed an optical sum-rule for insulators associated with a low-energy effective Hamiltonian in a variety of interacting “flat-band” systems hosting non-trivial band-geometry.

By focusing on solvable examples in the non-perturbative limit where the interaction scale overwhelms the bare kinetic energy, we have systematically disentangled the effects of emergent symmetries tied to the ground-state manifold and their band quantum geometry on the low-energy sum-rule. An interesting future direction is to extend these ideas to the realm of non-linear response functions and associated sum-rules [128].

Investigating the fate of these low-energy sum-rules in correlated Mott insulators, including those exhibiting fractionalization [129], remains an exciting frontier. For a variety of such quantum spin-liquid insulators with a finite charge-gap, the electrically neutral sub-gap excitations contribute to a power-law conductivity that vanishes in the limit of  $\omega \rightarrow 0$  [130–132]. The exact exponents depend on the dominant dissipation mechanism, and in the absence of any controlled analytical methods can be computed using the Ioffe-Larkin composition rule [133]. For example, there exist specific spin-liquid ground-states [131] where  $\text{Re}[\sigma_{xx}(\omega)] \sim (e^2 t^2 \omega^2 / h U^4)$ , where  $t$ ,  $U$  represent a characteristic hopping and interaction energy, respectively. Clearly, the low-energy absorption spectral weight restricted to frequencies comparable to the  $O(U)$  charge-gap will be finite, and will generically depend on the ratios of the microscopic energy-scales. The connections to any underlying quantum-geometry, which is often ignored in standard discussions of Mott insulators, remains an interesting future direction. It will be especially interesting to extend some of the ideas inspired by the study of quantum Hall-like wavefunctions to pursue this direction, without invoking standard parton-based Ioffe-Larkin based methods. On the experimental front, moiré materials present a unique platform to investigate these many-body phases [134], though measurements of their optical response in the energy window of interest remains an outstanding challenge.

We have also revealed an intriguing connection between a specific thermally regulated partial sum-rule and the quantum Fisher information. In the context of fermionic systems, the QFI has been argued to be a sensitive witness to multipartite entanglement [135, 136]. However, our explicit computations in the context of the partial sum-rules at low-temperatures, where the response either vanishes or is small even for ground-states with non-trivial entanglement (e.g. Laughlin-like states) demonstrate that the connection between multipartite entanglement and other metrics of entanglement (as measured via, e.g. entanglement entropies) is far from being obvious. This is not surprising given the distinct dependence on the density matrix for the different diagnostics of entanglement. Sharpening the underlying physical principles that describe the connections between measurable response functions in a restricted energy window, their underlying quantum geometry, and various metrics of quantum entanglement remains an exciting future research direction.

*Acknowledgements.*— DC thanks E. Berg, J. Dong, S. Kim, P. Ledwith, O. Lesser, Z. Papic, and A. Reddy for a

number of fruitful discussions. We thank J. Hofmann for his help in preparing Fig. 5. JFMV thanks Y. Kwan and J. Herzog-Arbeitman for fruitful discussions. The numerical computations in this work are supported in part by a NSF CAREER grant (DMR-2237522), and a Sloan Research Fellowship to DC. This research was supported in

part by grant NSF PHY-2309135 to the Kavli Institute for Theoretical Physics (KITP).

*Note added:* A recent manuscript has also proposed a connection between the UV sum-rule and quantum Fisher information [137]; the two manuscripts have minimal overlap.

- 
- [1] W. Kohn, Phys. Rev. **133**, A171 (1964).  
 [2] D. J. Scalapino, S. R. White, and S. Zhang, Phys. Rev. B **47**, 7995 (1993).  
 [3] I. Souza, T. Wilkens, and R. M. Martin, Phys. Rev. B **62**, 1666 (2000).  
 [4] P. Törmä, Phys. Rev. Lett. **131**, 240001 (2023).  
 [5] J. P. Provost and G. Vallee, Communications in Mathematical Physics **76**, 289 (1980).  
 [6] P. Törmä, S. Peotta, and B. A. Bernevig, Nature Reviews Physics **4**, 528 (2022).  
 [7] R. Roy, Phys. Rev. B **90**, 165139 (2014).  
 [8] S. A. Parameswaran, R. Roy, and S. L. Sondhi, Comptes Rendus. Physique **14**, 816 (2013).  
 [9] P. J. Ledwith, G. Tarnopolsky, E. Khalaf, and A. Vishwanath, Phys. Rev. Res. **2**, 023237 (2020).  
 [10] J. Ahn, G.-Y. Guo, and N. Nagaosa, Phys. Rev. X **10**, 041041 (2020).  
 [11] T. Holder, D. Kaplan, and B. Yan, Phys. Rev. Res. **2**, 033100 (2020).  
 [12] Q. Ma, A. G. Grushin, and K. S. Burch, Nature Materials **20**, 1601 (2021).  
 [13] G. E. Topp, C. J. Eckhardt, D. M. Kennes, M. A. Sentef, and P. Törmä, Phys. Rev. B **104**, 064306 (2021).  
 [14] J. Orenstein, J. Moore, T. Morimoto, D. Torchinsky, J. Harter, and D. Hsieh, Annual Review of Condensed Matter Physics **12**, 247 (2021).  
 [15] V. Kozii, A. Avdoshkin, S. Zhong, and J. E. Moore, Phys. Rev. Lett. **126**, 156602 (2021).  
 [16] J. Ahn, G.-Y. Guo, N. Nagaosa, and A. Vishwanath, Nature Physics **18**, 290 (2022).  
 [17] S. Chaudhary, C. Lewandowski, and G. Refael, Phys. Rev. Res. **4**, 013164 (2022).  
 [18] J. Mitscherling and T. Holder, Phys. Rev. B **105**, 085154 (2022).  
 [19] W. T. Tai and M. Claassen, Quantum-geometric light-matter coupling in correlated quantum materials (2023), arXiv:2303.01597 [cond-mat.str-el].  
 [20] P. C. Adak, S. Sinha, A. Agarwal, and M. M. Deshmukh, Nature Reviews Materials **9**, 481 (2024).  
 [21] R. C. McKay, F. Mahmood, and B. Bradlyn, Phys. Rev. X **14**, 011058 (2024).  
 [22] B. Bradlyn and P. Abbamonte, Spectral density and sum rules for second-order response functions (2024), arXiv:2404.16144 [cond-mat.mes-hall].  
 [23] N. Paul, Phys. Rev. B **109**, 085146 (2024).  
 [24] P. M. Tam, J. Herzog-Arbeitman, and J. Yu, arXiv e-prints , arXiv:2406.17023 (2024), arXiv:2406.17023 [cond-mat.mes-hall].  
 [25] X.-C. Wu, K.-L. Cai, M. Cheng, and P. Kumar, arXiv e-prints , arXiv:2408.16057 (2024), arXiv:2408.16057 [cond-mat.str-el].  
 [26] A. Kruchkov and S. Ryu, arXiv e-prints , arXiv:2408.10314 (2024), arXiv:2408.10314 [cond-mat.str-el].  
 [27] R. Resta and S. Sorella, Phys. Rev. Lett. **82**, 370 (1999).  
 [28] R. Resta, Phys. Rev. Lett. **96**, 137601 (2006).  
 [29] E. K. Kudinov, Sov. Phys. Solid State **33**, cond-mat/9902361 (1991), arXiv:cond-mat/9902361 [cond-mat.supr-con].  
 [30] Y. Onishi and L. Fu, Phys. Rev. X **14**, 011052 (2024).  
 [31] I. Souza, R. M. Martin, and M. Stengel, arXiv e-prints , arXiv:2407.17908 (2024), arXiv:2407.17908 [cond-mat.mtrl-sci].  
 [32] N. Batra and D. E. Feldman, arXiv e-prints , arXiv:2407.17603 (2024), arXiv:2407.17603 [cond-mat.mes-hall].  
 [33] N. Verma and R. Queiroz, arXiv e-prints , arXiv:2403.07052 (2024), arXiv:2403.07052 [cond-mat.mes-hall].  
 [34] N. Verma and R. Queiroz, arXiv e-prints , arXiv:2406.17845 (2024), arXiv:2406.17845 [cond-mat.mes-hall].  
 [35] Y. Onishi and L. Fu, arXiv e-prints , arXiv:2401.13847 (2024), arXiv:2401.13847 [cond-mat.str-el].  
 [36] R. Bistritzer and A. H. MacDonald, Proceedings of the National Academy of Sciences **108**, 12233 (2011), <https://www.pnas.org/content/108/30/12233.full.pdf>.  
 [37] N. Marzari and D. Vanderbilt, Phys. Rev. B **56**, 12847 (1997).  
 [38] P. Hyllus, W. Laskowski, R. Krischek, C. Schwemmer, W. Wiczczonek, H. Weinfurter, L. Pezzé, and A. Smerzi, Phys. Rev. A **85**, 022321 (2012).  
 [39] G. Tóth, Phys. Rev. A **85**, 022322 (2012).  
 [40] H. Strobel, W. Muessel, D. Linnemann, T. Zibold, D. B. Hume, L. Pezzé, A. Smerzi, and M. K. Oberthaler, Science **345**, 424 (2014), <https://www.science.org/doi/pdf/10.1126/science.1250147>.  
 [41] Y. Cao, V. Fatemi, A. Demir, S. Fang, S. L. Tomarken, J. Y. Luo, J. D. Sanchez-Yamagishi, K. Watanabe, T. Taniguchi, E. Kaxiras, R. C. Ashoori, and P. Jarillo-Herrero, Nature **556**, 80 (2018).  
 [42] Y. Cao, V. Fatemi, S. Fang, K. Watanabe, T. Taniguchi, E. Kaxiras, and P. Jarillo-Herrero, Nature **556**, 43 (2018).  
 [43] M. Yankowitz, S. Chen, H. Polshyn, Y. Zhang, K. Watanabe, T. Taniguchi, D. Graf, A. F. Young, and C. R. Dean, Science **363**, 1059 (2019).  
 [44] X. Lu, P. Stepanov, W. Yang, M. Xie, M. A. Aamir, I. Das, C. Urgell, K. Watanabe, T. Taniguchi, G. Zhang, A. Bachtold, A. H. MacDonald, and D. K. Efetov, Nature **574**, 653 (2019).  
 [45] J. M. Park, Y. Cao, K. Watanabe, T. Taniguchi, and P. Jarillo-Herrero, Nature **592**, 43 (2021).  
 [46] U. Zondiner, A. Rozen, D. Rodan-Legrain, Y. Cao, R. Queiroz, T. Taniguchi, K. Watanabe, Y. Oreg, F. von Oppen, A. Stern, and et al., Nature **582**, 203 (2020).

- [47] A. Uri, S. Grover, Y. Cao, J. A. Crosse, K. Bagani, D. Rodan-Legrain, Y. Myasoedov, K. Watanabe, T. Taniguchi, P. Moon, *et al.*, *Nature* **581**, 47 (2020).
- [48] Y. Saito, J. Ge, K. Watanabe, T. Taniguchi, and A. F. Young, *Nature Physics* **16**, 926 (2020).
- [49] Y. Saito, F. Yang, J. Ge, X. Liu, T. Taniguchi, K. Watanabe, J. Li, E. Berg, and A. F. Young, *Nature* **592**, 220 (2021).
- [50] Y. Cao, D. Rodan-Legrain, J. M. Park, N. F. Q. Yuan, K. Watanabe, T. Taniguchi, R. M. Fernandes, L. Fu, and P. Jarillo-Herrero, *Science* **372**, 264 (2021).
- [51] X. Liu, Z. Wang, K. Watanabe, T. Taniguchi, O. Vafek, and J. Li, *Science* **371**, 1261 (2021).
- [52] I. Das, X. Lu, J. Herzog-Arbeitman, Z.-D. Song, K. Watanabe, T. Taniguchi, B. A. Bernevig, and D. K. Efetov, *Nature Physics* **17**, 710 (2021).
- [53] A. Rozen, J. M. Park, U. Zondiner, Y. Cao, D. Rodan-Legrain, T. Taniguchi, K. Watanabe, Y. Oreg, A. Stern, E. Berg, *et al.*, *Nature* **592**, 214 (2021).
- [54] M. Serlin, C. L. Tschirhart, H. Polshyn, Y. Zhang, J. Zhu, K. Watanabe, T. Taniguchi, L. Balents, and A. F. Young, *Science* **367**, 900 (2020).
- [55] A. L. Sharpe, E. J. Fox, A. W. Barnard, J. Finney, K. Watanabe, T. Taniguchi, M. A. Kastner, and D. Goldhaber-Gordon, *Science* **365**, 605 (2019).
- [56] P. Stepanov, I. Das, X. Lu, A. Fahimniya, K. Watanabe, T. Taniguchi, F. H. L. Koppens, J. Lischner, L. Levitov, and D. K. Efetov, *Nature* **583**, 375 (2020).
- [57] S. Wu, Z. Zhang, K. Watanabe, T. Taniguchi, and E. Y. Andrei, *Nature Materials* **20**, 488 (2021).
- [58] Y. Saito, J. Ge, L. Rademaker, K. Watanabe, T. Taniguchi, D. A. Abanin, and A. F. Young, *Nature Physics* **17**, 478 (2021).
- [59] K. P. Nuckolls, R. L. Lee, M. Oh, D. Wong, T. Soejima, J. P. Hong, D. Călugăru, J. Herzog-Arbeitman, B. A. Bernevig, K. Watanabe, T. Taniguchi, N. Regnault, M. P. Zaletel, and A. Yazdani, Quantum textures of the many-body wavefunctions in magic-angle graphene (2023), arXiv:2303.00024 [cond-mat.mes-hall].
- [60] S. Grover, M. Bocarsly, A. Uri, P. Stepanov, G. D. Battista, I. Roy, J. Xiao, A. Y. Meltzer, Y. Myasoedov, K. Pareek, K. Watanabe, T. Taniguchi, B. Yan, A. Stern, E. Berg, D. K. Efetov, and E. Zeldov, *Nature Physics* **18**, 885 (2022).
- [61] J. Yu, B. A. Foutty, Z. Han, M. E. Barber, Y. Schattner, K. Watanabe, T. Taniguchi, P. Phillips, Z.-X. Shen, S. A. Kivelson, and B. E. Feldman, *Nature Physics* **18**, 825 (2022).
- [62] J. Yu, B. A. Foutty, Y. H. Kwan, M. E. Barber, K. Watanabe, T. Taniguchi, Z.-X. Shen, S. A. Parameswaran, and B. E. Feldman, Spin skyrmion gaps as signatures of intervalley-coherent insulators in magic-angle twisted bilayer graphene (2022).
- [63] E. Morissette, J.-X. Lin, D. Sun, L. Zhang, S. Liu, D. Rhodes, K. Watanabe, T. Taniguchi, J. Hone, J. Pollanen, M. S. Scheurer, M. Lilly, A. Mounce, and J. I. A. Li, Electron spin resonance and collective excitations in magic-angle twisted bilayer graphene (2022).
- [64] C.-C. Tseng, X. Ma, Z. Liu, K. Watanabe, T. Taniguchi, J.-H. Chu, and M. Yankowitz, *Nature Physics* **18**, 1038 (2022).
- [65] Y. Choi, J. Kemmer, Y. Peng, A. Thomson, H. Arora, R. Polski, Y. Zhang, H. Ren, J. Alicea, G. Refael, *et al.*, *Nature Physics* **15**, 1174 (2019).
- [66] M. Oh, K. P. Nuckolls, D. Wong, R. L. Lee, X. Liu, K. Watanabe, T. Taniguchi, and A. Yazdani, *Nature* **600**, 240 (2021).
- [67] K. P. Nuckolls, M. Oh, D. Wong, B. Lian, K. Watanabe, T. Taniguchi, B. A. Bernevig, and A. Yazdani, *Nature* **588**, 610 (2020).
- [68] Y. Xie, A. T. Pierce, J. M. Park, D. E. Parker, E. Khalaf, P. Ledwith, Y. Cao, S. H. Lee, S. Chen, P. R. Forrester, K. Watanabe, T. Taniguchi, A. Vishwanath, P. Jarillo-Herrero, and A. Yacoby, *Nature* **600**, 439 (2021).
- [69] J. Diez-Merida, A. Diez-Carlon, S. Y. Yang, Y. M. Xie, X. J. Gao, K. Watanabe, T. Taniguchi, X. Lu, K. T. Law, and D. K. Efetov, Magnetic Josephson junctions and superconducting diodes in magic angle twisted bilayer graphene (2021).
- [70] Y. Jiang, X. Lai, K. Watanabe, T. Taniguchi, K. Haule, J. Mao, and E. Y. Andrei, *Nature* **573**, 91 (2019).
- [71] H. S. Arora, R. Polski, Y. Zhang, A. Thomson, Y. Choi, H. Kim, Z. Lin, I. Z. Wilson, X. Xu, J.-H. Chu, K. Watanabe, T. Taniguchi, J. Alicea, and S. Nadj-Perge, *Nature* **583**, 379 (2020).
- [72] A. Kerelsky, L. J. McGilly, D. M. Kennes, L. Xian, M. Yankowitz, S. Chen, K. Watanabe, T. Taniguchi, J. Hone, C. Dean, *et al.*, *Nature* **572**, 95 (2019).
- [73] Y. Choi, H. Kim, Y. Peng, A. Thomson, C. Lewandowski, R. Polski, Y. Zhang, H. S. Arora, K. Watanabe, T. Taniguchi, *et al.*, *Nature* **589**, 536 (2021).
- [74] Y. Xie, B. Lian, B. Jäck, X. Liu, C.-L. Chiu, K. Watanabe, T. Taniguchi, B. A. Bernevig, and A. Yazdani, *Nature* **572**, 101 (2019).
- [75] D. Wong, K. P. Nuckolls, M. Oh, B. Lian, Y. Xie, S. Jeon, K. Watanabe, T. Taniguchi, B. A. Bernevig, and A. Yazdani, *Nature* **582**, 198 (2020).
- [76] A. T. Pierce, Y. Xie, J. M. Park, E. Khalaf, S. H. Lee, Y. Cao, D. E. Parker, P. R. Forrester, S. Chen, K. Watanabe, T. Taniguchi, A. Vishwanath, P. Jarillo-Herrero, and A. Yacoby, Unconventional sequence of correlated Chern insulators in magic-angle twisted bilayer graphene (2021), arXiv:2101.04123 [cond-mat.mes-hall].
- [77] G. Tarnopolsky, A. J. Kruchkov, and A. Vishwanath, *Phys. Rev. Lett.* **122**, 106405 (2019), publisher: American Physical Society.
- [78] N. Bultinck, E. Khalaf, S. Liu, S. Chatterjee, A. Vishwanath, and M. P. Zaletel, *Phys. Rev. X* **10**, 031034 (2020), publisher: American Physical Society.
- [79] B. Lian, Z.-D. Song, N. Regnault, D. K. Efetov, A. Yazdani, and B. A. Bernevig, *Phys. Rev. B* **103**, 205414 (2021).
- [80] Y. H. Kwan, G. Wagner, T. Soejima, M. P. Zaletel, S. H. Simon, S. A. Parameswaran, and N. Bultinck, *Phys. Rev. X* **11**, 041063 (2021).
- [81] T. Soejima, D. E. Parker, N. Bultinck, J. Hauschild, and M. P. Zaletel, *Phys. Rev. B* **102**, 205111 (2020).
- [82] Y. H. Kwan, Z. Wang, G. Wagner, S. H. Simon, S. A. Parameswaran, and N. Bultinck, Textured exciton insulators (2024), arXiv:2406.15343 [cond-mat.str-el].
- [83] Z. Wang, Y. H. Kwan, G. Wagner, S. H. Simon, N. Bultinck, and S. A. Parameswaran, Chern-textured exciton insulators with valley spiral order in moiré materials (2024), arXiv:2406.15342 [cond-mat.str-el].
- [84] J. F. Mendez-Valderrama, D. Mao, and D. Chowdhury,

- Low-energy optical sum-rule in moiré graphene (2023), arXiv:2312.03819 [cond-mat.str-el].
- [85] E. Tang, J.-W. Mei, and X.-G. Wen, Phys. Rev. Lett. **106**, 236802 (2011).
- [86] T. Neupert, L. Santos, C. Chamon, and C. Mudry, Phys. Rev. Lett. **106**, 236804 (2011).
- [87] N. Regnault and B. A. Bernevig, Phys. Rev. X **1**, 021014 (2011).
- [88] D. N. Sheng, Z.-C. Gu, K. Sun, and L. Sheng, Nature Communications **2**, 389 (2011).
- [89] L. Ju, A. H. MacDonald, K. F. Mak, J. Shan, and X. Xu, Nature Reviews Materials **9**, 455 (2024).
- [90] J. Cai, E. Anderson, C. Wang, X. Zhang, X. Liu, W. Holtzmann, Y. Zhang, F. Fan, T. Taniguchi, K. Watanabe, Y. Ran, T. Cao, L. Fu, D. Xiao, W. Yao, and X. Xu, Nature **622**, 63 (2023).
- [91] Y. Zeng, Z. Xia, K. Kang, J. Zhu, P. Knüppel, C. Vaswani, K. Watanabe, T. Taniguchi, K. F. Mak, and J. Shan, Nature **622**, 69 (2023).
- [92] F. Xu, Z. Sun, T. Jia, C. Liu, C. Xu, C. Li, Y. Gu, K. Watanabe, T. Taniguchi, B. Tong, J. Jia, Z. Shi, S. Jiang, Y. Zhang, X. Liu, and T. Li, Phys. Rev. X **13**, 031037 (2023).
- [93] Z. Lu, T. Han, Y. Yao, A. P. Reddy, J. Yang, J. Seo, K. Watanabe, T. Taniguchi, L. Fu, and L. Ju, Nature **626**, 759 (2024).
- [94] C. Repellin and T. Senthil, Phys. Rev. Res. **2**, 023238 (2020).
- [95] H. Li, U. Kumar, K. Sun, and S.-Z. Lin, Phys. Rev. Res. **3**, L032070 (2021).
- [96] P. Wilhelm, T. C. Lang, and A. M. Läuchli, Phys. Rev. B **103**, 125406 (2021).
- [97] Z. Liu and E. J. Bergholtz, in *Encyclopedia of Condensed Matter Physics (Second Edition)*, edited by T. Chakraborty (Academic Press, Oxford, 2024) second edition ed., pp. 515–538.
- [98] P. J. Ledwith, A. Vishwanath, and D. E. Parker, Phys. Rev. B **108**, 205144 (2023).
- [99] S. Kourtis, T. Neupert, C. Chamon, and C. Mudry, Phys. Rev. Lett. **112**, 126806 (2014).
- [100] A. G. Grushin, J. Motruk, M. P. Zaletel, and F. Pollmann, Phys. Rev. B **91**, 035136 (2015).
- [101] P. Sharma, Y. Peng, and D. N. Sheng, Phys. Rev. B **110**, 125142 (2024).
- [102] J. Yu, J. Herzog-Arbeitman, M. Wang, O. Vafek, B. A. Bernevig, and N. Regnault, Phys. Rev. B **109**, 045147 (2024).
- [103] Y. Sheffer and A. Stern, Phys. Rev. B **104**, L121405 (2021).
- [104] J. Wang, J. Cano, A. J. Millis, Z. Liu, and B. Yang, Phys. Rev. Lett. **127**, 246403 (2021).
- [105] J. Dong, P. J. Ledwith, E. Khalaf, J. Y. Lee, and A. Vishwanath, Phys. Rev. Res. **5**, 023166 (2023).
- [106] N. Morales-Durán, N. Wei, J. Shi, and A. H. MacDonald, Phys. Rev. Lett. **132**, 096602 (2024).
- [107] T. M. R. Wolf, Y.-C. Chao, A. H. MacDonald, and J. J. Su, arXiv e-prints , arXiv:2406.10709 (2024), arXiv:2406.10709 [cond-mat.str-el].
- [108] A. Abouelkomsan, N. Paul, A. Stern, and L. Fu, arXiv e-prints , arXiv:2403.14747 (2024), arXiv:2403.14747 [cond-mat.str-el].
- [109] W. Kohn, Phys. Rev. **123**, 1242 (1961).
- [110] S.-K. Yip, Phys. Rev. B **40**, 3682 (1989).
- [111] B. I. Halperin, P. A. Lee, and N. Read, Phys. Rev. B **47**, 7312 (1993).
- [112] S. M. Girvin, A. H. MacDonald, and P. M. Platzman, Phys. Rev. B **33**, 2481 (1986).
- [113] F. D. M. Haldane, Phys. Rev. Lett. **107**, 116801 (2011).
- [114] N. Read, Phys. Rev. B **58**, 16262 (1998).
- [115] P. Kumar and F. D. M. Haldane, Phys. Rev. B **106**, 075116 (2022).
- [116] D. Antoniou and A. H. MacDonald, Phys. Rev. B **46**, 15225 (1992).
- [117] F. Wu and A. H. MacDonald, Phys. Rev. B **94**, 241108 (2016).
- [118] J. Dong, J. Wang, and L. Fu, Dirac electron under periodic magnetic field: Platform for fractional chern insulator and generalized wigner crystal (2022), arXiv:2208.10516 [cond-mat.mes-hall].
- [119] B. Estienne, N. Regnault, and V. Crépel, Phys. Rev. Res. **5**, L032048 (2023).
- [120] B. Li and F. Wu, Variational mapping of chern bands to landau levels: Application to fractional chern insulators in twisted mote<sub>2</sub> (2024), arXiv:2405.20307 [cond-mat.mes-hall].
- [121] Y. Aharonov and A. Casher, Phys. Rev. A **19**, 2461 (1979).
- [122] B. Dubrovin and S. Novikov, Journal of Experimental and Theoretical Physics - J EXP THEOR PHYS **52** (1980).
- [123] D. Mao and D. Chowdhury, Phys. Rev. B **109**, 024507 (2024).
- [124] See supplementary material for additional details.
- [125] J. Wang, S. Klevtsov, and Z. Liu, Physical Review Research **5**, 023167 (2023).
- [126] F. Wu, T. Lovorn, E. Tutuc, I. Martin, and A. H. MacDonald, Phys. Rev. Lett. **122**, 086402 (2019).
- [127] J. S. Hofmann, E. Berg, and D. Chowdhury, Phys. Rev. Lett. **130**, 226001 (2023).
- [128] H. Watanabe and M. Oshikawa, Phys. Rev. B **102**, 165137 (2020).
- [129] C. Broholm, R. J. Cava, S. A. Kivelson, D. G. Nocera, M. R. Norman, and T. Senthil, Science **367**, eaay0668 (2020), <https://www.science.org/doi/pdf/10.1126/science.aay0668>.
- [130] T.-K. Ng and P. A. Lee, Phys. Rev. Lett. **99**, 156402 (2007).
- [131] A. C. Potter, T. Senthil, and P. A. Lee, Phys. Rev. B **87**, 245106 (2013).
- [132] Y. Huh, M. Punk, and S. Sachdev, Phys. Rev. B **87**, 235108 (2013).
- [133] L. B. Ioffe and A. I. Larkin, Phys. Rev. B **39**, 8988 (1989).
- [134] T. Li, S. Jiang, L. Li, Y. Zhang, K. Kang, J. Zhu, K. Watanabe, T. Taniguchi, D. Chowdhury, L. Fu, J. Shan, and K. F. Mak, Nature **597**, 350 (2021).
- [135] P. Hauke, M. Heyl, L. Tagliacozzo, and P. Zoller, Nature Physics **12**, 778 (2016).
- [136] R. Costa de Almeida and P. Hauke, Phys. Rev. Res. **3**, L032051 (2021).
- [137] D. Balut, B. Bradlyn, and P. Abbamonte, arXiv e-prints , arXiv:2409.15583 (2024), arXiv:2409.15583 [cond-mat.mes-hall].
- [138] E. Cancés and C. Le Bris, International Journal of Quantum Chemistry **79**, 82 (2000).
- [139] D. Parker, P. Ledwith, E. Khalaf, T. Soejima, J. Hauschild, Y. Xie, A. Pierce, M. P. Zaletel, A. Yacoby, and A. Vishwanath, Field-tuned and zero-field

fractional chern insulators in magic angle graphene (2021), arXiv:2112.13837 [cond-mat.str-el].

[140] J. K. Jain, Phys. Rev. B **40**, 8079 (1989).

[141] J. K. Jain, Advances in Physics **41**, 105 (1992),

<https://doi.org/10.1080/00018739200101483>.

[142] X.-G. Wen, Int. J. Mod. Phys. B **6**, 1711 (1992).

### A. Lehmann representation for optical sum-rules

In this appendix, we express the partial sum rule in Eq. 4 for the longitudinal conductivity at temperature  $T \ll E_{\text{gap}}$  and  $\Lambda$  inside the bandgap to the remote bands. In the spectral representation, the real part of the longitudinal conductivity can be written as,

$$\text{Re}[\sigma_{\text{xx}}^{\text{eff}}(q_x \rightarrow 0, \omega)] = \frac{\pi e^2}{\omega} \sum_{m,n} \frac{e^{-\beta E_n} - e^{-\beta E_m}}{Z} \langle n | j_x^{\text{eff}}(q_x \rightarrow 0) | m \rangle \langle m | j_x^{\text{eff}}(-q_x \rightarrow 0) | n \rangle \delta(\omega - E_m + E_n), \quad (\text{A1})$$

where  $Z$  is the partition function. If we perform an integral over  $\omega$ , at temperature  $T \ll E_{\text{gap}}$ , for  $|\omega| \lesssim E_{\text{gap}}$ , we only need to consider the many-body states  $|n\rangle$  and  $|m\rangle$  that belong to the low-energy projected Hilbert space  $\mathbb{H}$  with eigen-energies  $E_n$ ,  $E_m$ , and therefore,

$$\begin{aligned} \int_0^\Lambda d\omega \frac{\text{Re}[\sigma_{\text{xx}}^{\text{eff}}(q_x \rightarrow 0, \omega)]}{\omega} &\approx \pi e^2 \sum_{m,n \in \mathbb{H}} \langle n | j_x^{\text{eff}}(q_x \rightarrow 0) | m \rangle \langle m | j_x^{\text{eff}}(-q_x \rightarrow 0) | n \rangle \frac{e^{-\beta E_n} - e^{-\beta E_m}}{Z(E_m - E_n)^2} \theta(E_m - E_n) \\ &= -\pi e^2 \sum_{m,n \in \mathbb{H}} \langle n | [\hat{X}, H] | m \rangle \langle m | [\hat{X}, H] | n \rangle \frac{e^{-\beta E_n} - e^{-\beta E_m}}{Z(E_m - E_n)^2} \theta(E_m - E_n) \\ &= \pi e^2 \sum_{m,n \in \mathbb{H}} \langle n | \hat{X} | m \rangle \langle m | \hat{X} | n \rangle \frac{e^{-\beta E_n} - e^{-\beta E_m}}{Z} \theta(E_m - E_n). \end{aligned} \quad (\text{A2})$$

Importantly, since the many-body states are restricted only to  $\mathbb{H}$ , the matrix-elements above are associated with the projected position coordinate,  $\hat{X} \rightarrow \hat{\bar{X}}$ .

### B. Details of Hartree-Fock calculations for MATBG

For all calculations in the symmetry broken insulators of TBG, we start by determining the ground state by self-consistent Hartree-Fock using the optimal damping algorithm [138] to speed up convergence, and initialize the Hartree-Fock Projector  $\mathcal{P}$  by filling up the states of a random quadratic Hamiltonian. This is done in parallel using 128 random seeds, and the minimum-energy self-consistent solution is selected to be the ground-state. For all the calculations we used the ‘‘average’’ subtraction scheme [80, 139] with  $\theta = 1.08$  and  $\kappa = 0.75$ . For the results in Fig. 2a, the calculations for the bound,  $\bar{\mathbb{S}}/\Delta$ , are taken from [84] which were performed on a  $12 \times 12$  system due to the complexity involved in calculating  $\bar{\mathbb{S}}$  which involves various derivatives of projectors whose dimension scales with the plane-wave cutoff of the continuum model. For details on the calculation of  $\bar{\mathbb{S}}$  see the supplementary information of [84]. The calculations of the MBPQM and the structure factor in Fig. 2 were performed on a  $24 \times 24$  system. For  $\varepsilon > 0.1$ , the Hartree-Fock ground state is found to be a spin-unpolarized IKS close to a momentum  $\mathbf{q}_{IKS} = 2\mathbf{M}/3$  (within the resolution of our grid), with  $\mathbf{M}$  being the M-point of the MBZ [80]. For  $\varepsilon < 0.1$ , the solution is instead a spin-polarized KIVC state. To achieve lower energy solutions that improve the convergence of  $\text{tr}[G_{\text{xx}}(\mathbf{k})]$ , we ran the HF loop starting from the ground state of either a spin diagonal, or a spin-independent random Hamiltonian for  $\varepsilon < 0.1$ , and  $\varepsilon > 0.1$ , respectively. Once the ground-state reduced density matrix is obtained, the projected spectral weight is computed using the projected structure factor (quantum weight), as detailed in Appendix C. We explicitly avoid the region of the phase diagram near the first order transition between KIVC and IKS since the exact location of the transition is dependent on the subtraction scheme, and instead we focused primarily deep in the two phases. Near the transition point, the indirect gap on the KIVC side is also reduced drastically from its value at zero strain (with a strong tendency towards semi-metallic behavior).

### C. Projected quantum weight for interacting Slater determinant states

Since the projected quantum weight is related to the long wavelength behavior of the projected structure factor, we can evaluate it directly by simply expanding  $\bar{\mathcal{S}}(\mathbf{q})$  around small  $\mathbf{q}$ . For a Slater determinant state, such as the Hartree-Fock mean-field solution for TBG with projected Coulomb interactions at integer fillings, the projected structure factor can then be easily obtained via Wick's theorem:

$$\begin{aligned}\bar{\mathcal{S}}(\mathbf{q}) &= \sum_{\mathbf{k}, \mathbf{k}'} \langle c_{\mathbf{k}, \alpha}^\dagger c_{\mathbf{k}-\mathbf{q}, \beta} \lambda_{\alpha\beta}(\mathbf{k}, \mathbf{q}) c_{\mathbf{k}', \alpha'}^\dagger c_{\mathbf{k}'+\mathbf{q}, \beta'} \lambda_{\alpha'\beta'}(\mathbf{k}', -\mathbf{q}) \rangle - \langle c_{\mathbf{k}, \alpha}^\dagger c_{\mathbf{k}-\mathbf{q}, \beta} \lambda_{\alpha\beta}(\mathbf{k}, \mathbf{q}) \rangle \langle c_{\mathbf{k}', \alpha'}^\dagger c_{\mathbf{k}'+\mathbf{q}, \beta'} \lambda_{\alpha'\beta'}(\mathbf{k}', -\mathbf{q}) \rangle \\ &= \sum_{\mathbf{k}, \mathbf{k}'} \langle c_{\mathbf{k}, \alpha}^\dagger c_{\mathbf{k}'+\mathbf{q}, \beta'} \rangle \langle c_{\mathbf{k}-\mathbf{q}, \beta} c_{\mathbf{k}', \alpha'}^\dagger \rangle \lambda_{\alpha\beta}(\mathbf{k}, \mathbf{q}) \lambda_{\alpha'\beta'}(\mathbf{k}', -\mathbf{q})\end{aligned}\quad (\text{C1a})$$

$$= \sum_{\mathbf{k}, \mathbf{k}'} \text{Tr} \left\{ \hat{\lambda}(\mathbf{k}, \mathbf{q}) \left\{ \mathbf{1} \delta_{\mathbf{k}', \mathbf{k}-\mathbf{q}} - [\mathcal{P}(\mathbf{k}', \mathbf{k}-\mathbf{q})]^T \right\} \hat{\lambda}(\mathbf{k}', -\mathbf{q}) [\mathcal{P}(\mathbf{k}, \mathbf{k}'+\mathbf{q})]^T \right\}, \quad (\text{C1b})$$

where the trace is taken over the band, orbital and spin indices of the projected bands, respectively, and  $\mathcal{P}(\mathbf{k}, \mathbf{k}')$  is the one-particle reduced density matrix, whose matrix elements are given by

$$[\mathcal{P}(\mathbf{k}, \mathbf{k}')]_{\alpha\beta} = \langle c_{\mathbf{k}, \alpha}^\dagger c_{\mathbf{k}', \beta} \rangle. \quad (\text{C2})$$

Note that for mean-field states that are generalized FM states in the orbital basis at each  $\mathbf{k}$  point, the structure factor can be considerably simplified; this includes e.g. the IVC ordering in TBG, as well as the IKS states. For these generalized FM states, the wavefunction is an eigenstate of the projected particle number operator at “each”  $\mathbf{k}$  point, namely,

$$c_{\mathbf{k}, \alpha}^\dagger c_{\mathbf{k}, \alpha} |\Psi_{FM}\rangle = \nu |\Psi_{FM}\rangle, \quad (\text{C3})$$

where  $\nu$  is the filling factor. For IKS, we simply replace  $\mathbf{k}$  by  $\tilde{\mathbf{k}} = \mathbf{k} - \mathbf{Q}\tau_z/2$ , where  $\mathbf{Q}$  is the ordering wave vector for IKS and  $\tau_z$  denotes the Pauli matrix in valley space.

From Eq.C3, the following holds,

$$\langle \Psi_{FM} | c_{\mathbf{k}, \alpha}^\dagger c_{\mathbf{k}, \alpha} c_{\mathbf{k}', \beta}^\dagger c_{\mathbf{k}'', \gamma} | \Psi_{FM} \rangle - \langle \Psi_{FM} | c_{\mathbf{k}, \alpha}^\dagger c_{\mathbf{k}, \alpha} | \Psi_{FM} \rangle \langle \Psi_{FM} | c_{\mathbf{k}', \beta}^\dagger c_{\mathbf{k}'', \gamma} | \Psi_{FM} \rangle = 0 \quad (\text{C4})$$

$$\Leftrightarrow \langle \Psi_{FM} | c_{\mathbf{k}, \alpha}^\dagger c_{\mathbf{k}'', \gamma} | \Psi_{FM} \rangle \langle \Psi_{FM} | c_{\mathbf{k}, \alpha} c_{\mathbf{k}', \beta}^\dagger | \Psi_{FM} \rangle = 0, \quad (\text{C5})$$

where  $\mathbf{k}', \beta$  and  $\mathbf{k}'', \gamma$  are arbitrary.

Also, for the generalized FM states (excluding IKS),

$$\mathcal{P}(\mathbf{k}, \mathbf{k}') \equiv \delta_{\mathbf{k}, \mathbf{k}'} \hat{P}_{\mathbf{k}}, \quad (\text{C6})$$

while for IKS, we have

$$\mathcal{P}(\mathbf{k}, \mathbf{k}') \equiv \delta_{\mathbf{k}, \tilde{\mathbf{k}}+\mathbf{Q}\tau_z/2} \delta_{\mathbf{k}', \tilde{\mathbf{k}}+\mathbf{Q}\tau_z/2} \hat{P}_{\tilde{\mathbf{k}}}. \quad (\text{C7})$$

Therefore, from Eq.C5 we have  $(\mathbf{1} - \hat{P}_{\mathbf{k}})\hat{P}_{\mathbf{k}} = 0$  and  $(\mathbf{1} - \hat{P}_{\tilde{\mathbf{k}}})\hat{P}_{\tilde{\mathbf{k}}} = 0$ .

From the above equations, it is readily seen that for the generalized FM states in TBG, the terms in  $\bar{\mathcal{S}}(\mathbf{q})$  vanish if  $\alpha = \beta$  or  $\alpha' = \beta'$  and the corresponding  $\mathbf{q} = 0$  for the fermion operators.

Therefore, when we expand around  $\mathbf{q}$ , the leading order terms in  $\mathbf{q}$  vanish. For the  $q^2$ - contribution, the terms involving double derivatives of the form-factor vanishes. To conclude, for generalized FM states,

$$\bar{\mathcal{S}}(\mathbf{q}) = q_\mu q_\nu \sum_{\mathbf{k}} \text{Tr} \left\{ \left[ \overrightarrow{\partial}_\mu - i\hat{A}_{\mathbf{k}, \mu} \right] \left\{ \mathbf{1} - [\hat{P}_{\mathbf{k}}]^T \right\} \left[ \overleftarrow{\partial}_\nu + i\hat{A}_{\mathbf{k}', \nu} \right] [\hat{P}_{\mathbf{k}}]^T \right\}, \quad (\text{C8})$$

where the arrows over the derivatives denote the direction of taking derivative, i.e., they all act on the  $\left\{ \mathbf{1} - [\hat{P}_{\mathbf{k}}]^T \right\}$  term. For the IKS states, note that the form factor is always diagonal in valley, we arrive at the same expression as in Eq.C8 but with  $\mathbf{k}$  replaced by  $\tilde{\mathbf{k}}$ .

Alternatively, we can calculate the same  $\bar{\mathcal{S}}(\mathbf{q})$  in a new basis where the HF Hamiltonian is diagonalized.  $H_{MF} = \sum_{\mathbf{k}, m} \tilde{\epsilon}_{\mathbf{k}, m} \tilde{c}_{m, \mathbf{k}}^\dagger \tilde{c}_{m, \mathbf{k}}$ , where  $m$  labels the HF bands. The HF approximation is done by projecting the Hamiltonian to the low-energy, with the same energy cut-off that  $\bar{\mathcal{S}}(\mathbf{q})$  is evaluated within.

In the new basis,

$$\bar{S}(\mathbf{q}) = \sum_{\mathbf{k}, \mathbf{k}'} \langle \tilde{c}_{m, \mathbf{k}}^\dagger \tilde{c}_{n', \mathbf{k}'+\mathbf{q}} \rangle \langle \tilde{c}_{n, \mathbf{k}-\mathbf{q}} \tilde{c}_{m', \mathbf{k}'}^\dagger \rangle \tilde{\lambda}_{mn}(\mathbf{k}, \mathbf{q}) \tilde{\lambda}_{m'n'}(\mathbf{k}', -\mathbf{q}) \quad (\text{C9a})$$

$$= \sum_{\mathbf{k}, m \in \text{occ}, n \notin \text{occ}} \tilde{\lambda}_{mn}(\mathbf{k}, \mathbf{q}) \tilde{\lambda}_{nm}(\mathbf{k} - \mathbf{q}, -\mathbf{q}) \quad (\text{C9b})$$

$$= q_\mu q_\nu \sum_{\mathbf{k}, m \in \text{occ}} \langle \partial_\mu \tilde{u}_{m, \mathbf{k}} | (\mathcal{P}_{\text{IR}}(\mathbf{k}) - \mathcal{P}_{\text{occ}}(\mathbf{k})) | \partial_\nu \tilde{u}_{m, \mathbf{k}} \rangle + (\mu \leftrightarrow \nu), \quad (\text{C9c})$$

where  $\mathcal{P}_{\text{IR}}(\mathbf{k}) = \sum_{m \in \text{IR}} |\tilde{u}_{m, \mathbf{k}}\rangle \langle \tilde{u}_{m, \mathbf{k}}|$  sums over all the low-energy bands that the HF Hamiltonian keeps, and  $\mathcal{P}_{\text{occ}}(\mathbf{k}) = \sum_{m \in \text{occ}} |\tilde{u}_{m, \mathbf{k}}\rangle \langle \tilde{u}_{m, \mathbf{k}}|$  is the projection to the occupied HF bands. For IKS states, the above expression holds by replacing  $\mathbf{k}$  with  $\tilde{\mathbf{k}}$ . Note that the above formula can also be generalized to Slater determinant of CDW insulators, by considering the Bloch wavefunction in the reduced BZ of the enlarged unitcell.

Therefore, we can define a ‘‘projected’’ quantum geometric tensor,

$$G_{\mu\nu}^{mn}(\mathbf{k}) = \langle \partial_\mu \tilde{u}_{m, \mathbf{k}} | (\mathcal{P}_{\text{IR}}(\mathbf{k}) - \mathcal{P}_{\text{occ}}(\mathbf{k})) | \partial_\nu \tilde{u}_{n, \mathbf{k}} \rangle, \quad (\text{C10})$$

which takes into account only the ‘‘low-energy’’ part contribution to the quantum geometry and is related to the fluctuation of the ‘‘projected’’ position operator.

To evaluate the projected quantum geometric tensor, we perform a finite difference evaluation of Eq. C10. First we evaluate the metric by setting  $m = n$  and  $\mu = \nu = x$ . In this case, we approximate the derivative of the states by  $|\partial_{k_x} u_{n\mathbf{k}}\rangle \approx [|u_{n\mathbf{k}+\delta k_x}\rangle - |u_{n\mathbf{k}}\rangle] / \delta k_x$ , which results in the following expression for the metric in terms of the finite differences of the form factor [82]:

$$G_{xx}^{nn}(\mathbf{k}) = \frac{1}{\delta k_x^2} \left( \sum_{\ell \in \text{IR}} |\langle u_{n\mathbf{k}+\delta k_x} | u_{\ell\mathbf{k}} \rangle|^2 - \sum_{\ell \in \text{occ}} |\langle u_{n\mathbf{k}+\delta k_x} | u_{\ell\mathbf{k}} \rangle|^2 \right). \quad (\text{C11})$$

When evaluating this expression in the Hartree-Fock ground states of TBG, we calculate  $G_{xx}^{nn}$  by performing a unitary transformation on the form factors of TBG determined by the eigenstates of the self-consistent Hartree-Fock Hamiltonian. Since the intervalley form factor is parametrically smaller than the intravalley form factor at small angles, the rotation neglects valley mixing. Finally, when comparing to the projected quantum weight, we compute the trace over occupied orbitals in the symmetry broken phase, given by:

$$\text{Tr}[G_{xx}] = \frac{1}{V} \sum_{\mathbf{k}} \sum_{\ell \in \text{occ}} G_{xx}^{\ell\ell}(\mathbf{k}). \quad (\text{C12})$$

#### D. Emergent guiding center coordinate in LLL under periodic magnetic field

Recall that for a spinless LLL under a uniform magnetic field, we can choose a set of orthonormal basis  $|n\rangle$  on the plane,

$$\psi_n(\mathbf{r}) = \langle \mathbf{r} | n \rangle = R_n^{-1} z^n e^{-\frac{|z|^2}{4}}, \quad (\text{D1})$$

where  $R_n = \sqrt{\pi 2^{n+1} n!}$  is the normalization factor.

Therefore, in the  $|n\rangle$  basis, the matrix elements of the projected position operator can be written as,

$$\langle l | \hat{X} | n \rangle = \frac{1}{\sqrt{2}} [\delta_{l, n+1} \sqrt{n+1} + \delta_{l, n-1} \sqrt{n}] \quad (\text{D2})$$

$$\langle l | \hat{Y} | n \rangle = \frac{1}{\sqrt{2}i} [\delta_{l, n+1} \sqrt{n+1} - \delta_{l, n-1} \sqrt{n}]. \quad (\text{D3})$$

Hence, we can write  $\hat{X}$  acting on the wavefunctions as,

$$\hat{X} \psi_n(\mathbf{r}) = \frac{1}{2} \left[ z + 2\partial_z + \frac{\bar{z}}{2} \right] \varphi_n(\mathbf{r}), \quad (\text{D4})$$



and similarly for  $\hat{Y}$ .

Equivalently, we can write  $\hat{X}$  in the second quantized language. We define the creation operator  $c_n^\dagger$  as creating a particle in state  $|n\rangle$ ,

$$\hat{X} = \frac{1}{\sqrt{2}} \sum_n \left( \sqrt{n+1} c_{n+1}^\dagger c_n + \sqrt{n} c_{n-1}^\dagger c_n \right). \quad (\text{D5})$$

For a completely filled LL denoted  $|\Psi_{\nu=1}\rangle$ , the projected position operator annihilates the state in the thermodynamic limit due to the full occupation of the single-particle orbitals of the LL. For a finite system with open boundary conditions, we need to truncate the Hilbert space to  $|n_{\max}\rangle = |N_\phi - 1\rangle$ , where  $2\pi N_\phi$  is the total magnetic flux, such that there is one orbital per magnetic flux; the thermodynamic limit is approached for  $N \rightarrow \infty$ . With the truncation for a finite particle number, we can justify that  $\hat{X}|\Psi_{\nu=1}\rangle = 0$ , which is also the Laughlin state with  $m = 1$ . In fact, for any Laughlin wavefunction,  $\hat{X}|\Psi_L\rangle = 0$  holds. We will come back to this in more detail using parton construction when we discuss the generalized Laughlin states under a periodic magnetic field.

Let us now consider the LLL under a periodic magnetic field. We can still define a set of complete and independent eigenvectors  $|n_s\rangle$ ,

$$\psi_{n_s}(\mathbf{r}) = \langle \mathbf{r} | n_s \rangle = R_n^{-1} z^n e^{-\frac{|z|^2}{4} - \tilde{\varphi}(\mathbf{r})}, \quad (\text{D6})$$

where  $\tilde{\varphi}(\mathbf{r}) = -\frac{\phi_1}{|G|^2} \sum_j e^{i\mathbf{k}_j \cdot \mathbf{r}}$  and  $|G|$  is the norm of the reciprocal lattice vector  $\mathbf{k}_j$ 's. For a non-vanishing  $\phi_1$ , the  $|n_s\rangle$  are not normalized and different  $|n_s\rangle$ 's are non-orthogonal.

Since  $|n_s\rangle$ 's are independent and form a complete basis, we can still define a projector  $\mathcal{P}$ ,

$$\mathcal{P} = \sum_{l,n} |l_s\rangle \langle l_n| (\hat{O}^{-1})_{ln} \langle n_s|, \quad (\text{D7})$$

where  $\hat{O}_{ln} = \langle l_s | n_s \rangle$  is the overlapping matrix. Since  $\hat{O}$  is Hermitian by definition, as long as  $\hat{O}$  is positive definite, we can always diagonalize  $\hat{O}$  as,

$$(\hat{O}^{-1})^T = \hat{A}^\dagger \hat{A}. \quad (\text{D8})$$

We can find  $\hat{A}$  perturbatively in  $\phi_1$  and

$$|\tilde{n}\rangle = \sum_l \hat{A}_{nl} |l_s\rangle = |n\rangle + \frac{\phi_1}{|G|^2} \sum_j (1 - |l\rangle \langle l|) e^{i\mathbf{k}_j \cdot \mathbf{r}} |n\rangle + O(\phi_1^2), \quad (\text{D9})$$

defines an orthonormal basis and the projector can be written as  $\mathcal{P} = \sum_n |\tilde{n}\rangle \langle \tilde{n}|$ .

Now let us consider the projected density operators:

$$\hat{\rho}_{\mathbf{q}} = \mathcal{P} e^{i\mathbf{q} \cdot \mathbf{r}} \mathcal{P} = \sum_{l,n} |\tilde{l}\rangle \langle \tilde{l}| e^{i\mathbf{q} \cdot \mathbf{r}} |\tilde{n}\rangle \langle \tilde{n}| \quad (\text{D10})$$

$$= \sum_{l,n} |\tilde{l}\rangle \left( \hat{\rho}_{\mathbf{q}}^0 \right)_{ln} \langle \tilde{n}| + \frac{\phi_1}{|G|^2} \sum_{l,n,j} |\tilde{l}\rangle \left[ 2\hat{\rho}_{\mathbf{q}+\mathbf{k}_j}^0 - \hat{\rho}_{\mathbf{q}}^0 \hat{\rho}_{\mathbf{k}_j}^0 - \hat{\rho}_{\mathbf{k}_j}^0 \hat{\rho}_{\mathbf{q}}^0 \right]_{ln} \langle \tilde{n}| + O(\phi_1^2) \quad (\text{D11})$$

$$\equiv \hat{\rho}_{\mathbf{q}}^0 + \frac{\phi_1}{|G|^2} \sum_j \hat{\rho}_{\mathbf{q}+\mathbf{k}_j}^0 \left[ 2 - e^{\frac{\bar{q}k_j}{2}} - e^{\frac{qk_j}{2}} \right] + O(\phi_1^2), \quad (\text{D12})$$

where  $\left( \hat{\rho}_{\mathbf{q}}^0 \right)_{ln} \equiv \langle l | e^{i\mathbf{q} \cdot \mathbf{r}} | n \rangle$  is the matrix element of the density operator of the LLL under uniform field, which satisfies the GMP algebra,  $\left( \hat{\rho}_{\mathbf{q}_1}^0 \hat{\rho}_{\mathbf{q}_2}^0 \right)_{ln} = e^{\frac{\bar{q}_1 \bar{q}_2}{2}} \left( \hat{\rho}_{\mathbf{q}_1 + \mathbf{q}_2}^0 \right)_{ln}$ . Therefore  $\sum_{l,n} |\tilde{l}\rangle \left( \hat{\rho}_{\mathbf{q}}^0 \right)_{ln} \langle \tilde{n}| \equiv \hat{\rho}_{\mathbf{q}}^0$  are operators acting on the states of the LLL under *periodic* magnetic field that also satisfy GMP algebra. Hence, in the  $\mathbf{q} \rightarrow 0$  limit, we call the linear in  $\mathbf{q}$  term derived from  $\hat{\rho}_{\mathbf{q}}^0$  the ‘‘emergent’’ guiding center coordinates  $\hat{X}_{\mu,0}$  since they satisfy the same algebra as the guiding center coordinates of the LLL under uniform field (for an equivalent definition written in momentum space basis, see Ref. [125]). In the  $|\tilde{n}\rangle$  basis, we have,

$$\hat{X}_0 = \sum_{l,n} |\tilde{l}\rangle \langle l | \hat{X} | n \rangle \langle \tilde{n}| = \frac{1}{\sqrt{2}} \sum_n \left[ \sqrt{n+1} |\widetilde{n+1}\rangle \langle \tilde{n}| + \sqrt{n} |\widetilde{n-1}\rangle \langle \tilde{n}| \right]. \quad (\text{D13})$$

Therefore, if we consider a many-body state at  $\nu = 1$  of the LLL under periodic magnetic field,

$$|\Psi_{\nu=1}\rangle = \tilde{R}^{-1} \prod_{n=0}^{n_{\max}} \tilde{c}_n^\dagger |0\rangle, \quad (\text{D14})$$

where  $\tilde{c}_n^\dagger$  creates particle with orbital  $|\tilde{n}\rangle$  and  $\tilde{R}$  is the normalization factor. It is readily seen that  $\hat{X}_0 |\Psi_{\nu=1}\rangle = 0$ . Now let us expand  $\tilde{c}_n$  in the  $|n_s\rangle$  basis. In this case, due to the uniqueness of the  $\nu = 1$  state, we also have,

$$|\Psi_{\nu=1}\rangle = R^{-1} \prod_{n=0}^{n_{\max}} c_{n_s}^\dagger |0\rangle, \quad (\text{D15})$$

where  $c_{n_s}^\dagger$  creates particle with orbital  $|n_s\rangle$  and  $R$  is another normalization factor. Hence in real space, we can write the wavefunction as,

$$\Psi_{\nu=1}(\mathbf{r}_1, \dots, \mathbf{r}_N) = R^{-1} \prod_{i<j} (z_i - z_j) e^{-\sum_i \frac{|z_i|^2}{4} - \tilde{\varphi}(\mathbf{r}_i)}. \quad (\text{D16})$$

Now let us discuss the generalized Laughlin states,

$$\Psi_{gL}(\mathbf{r}_1, \dots, \mathbf{r}_N) = R_g^{-1} \prod_{i<j} (z_i - z_j)^m e^{-\sum_i \frac{|z_i|^2}{4} - \tilde{\varphi}(\mathbf{r}_i)}. \quad (\text{D17})$$

Again, one can view  $\Psi_{gL}$  as  $m$  copies of  $\Psi_{\nu=1}$ , with particle number  $N = \frac{N_\phi}{m}$  and with magnetic field  $\frac{B(\mathbf{r})}{m}$ , namely,

$$\Psi_{gL}(\mathbf{r}_1, \dots, \mathbf{r}_N) = R_g^{-1} \int \prod_{i=1}^N \prod_{l=1}^m d\mathbf{r}_{i,\alpha_l} \delta(\mathbf{r}_i - \mathbf{r}_{i,\alpha_l}) \prod_{i<j} (z_{i,\alpha_l} - z_{j,\alpha_l}) e^{-\sum_i \frac{|z_{i,\alpha_l}|^2}{4m} - \frac{\tilde{\varphi}(\mathbf{r}_{i,\alpha_l})}{m}}, \quad (\text{D18})$$

where  $\alpha_j$  labels different copies.

This treatment of the Laughlin state is equivalent to a parton construction, where the physical fermion is fractionalized into  $m$  species of fermions [140–142]. To be explicit, we can write the generalized Laughlin wave function in terms of the parton fields as,

$$|\Psi_{gL}\rangle \propto \mathcal{P}_g \prod_{l=1}^m \prod_{n=0}^{n_{\max}} \tilde{c}_{\alpha_l, n}^\dagger |0\rangle, \quad (\text{D19})$$

where the  $\propto$  means the LHS and RHS can differ by a normalization constant. We enlarge the Hilbert space to  $m$  copies of LLL, labelled by  $\alpha_l$ , each of which has  $n_{\max} = \frac{N_\phi}{m} - 1$ , and  $\mathcal{P}_g$  introduces the Guzwiller projection to the physical Hilbert space,

$$\langle \mathbf{X} | \mathcal{P}_g | \mathbf{X}_{\alpha_1}, \dots, \mathbf{X}_{\alpha_m} \rangle = \prod_{l=1}^m \delta(\mathbf{X} - \mathbf{X}_{\alpha_l}), \quad (\text{D20})$$

where  $\mathbf{X}$  is a shorthand notation for the coordinates of  $N$  particles,  $\mathbf{x}_1, \dots, \mathbf{x}_N$ .

In order to evaluate the action of  $\hat{X}_0$  on the generalized Laughlin state, we introduce an auxillary operator  $\hat{\tilde{X}}_0$  acting on the enlarged Hilbert space such that

$$\hat{\tilde{X}}_0 = \mathcal{P}_g \hat{X}_0. \quad (\text{D21})$$

Note that the choice of  $\hat{\tilde{X}}_0$  is not unique due to the gauge redundancy in the parton construction. A convenient choice for our purpose is to let,

$$\hat{\tilde{X}}_0 = \frac{1}{\sqrt{2}} \sum_n \left[ \sqrt{n+1} \tilde{c}_{\alpha_1, n+1}^\dagger \tilde{c}_{\alpha_1, n} + \sqrt{n} \tilde{c}_{\alpha_1, n-1}^\dagger \tilde{c}_{\alpha_1, n} \right] \otimes \prod_{l \neq 1} \mathbb{I}_{\alpha_l}, \quad (\text{D22})$$

where  $\hat{\tilde{X}}_0$  only acts non-trivially on  $\alpha_1$  but acts trivially on all the other species.

Since  $\hat{\tilde{X}}_0 \prod_{n=0}^{n_{\max}} \tilde{c}_{\alpha_1, n}^\dagger |0\rangle = 0$  due to the full occupation of the orbitals of the  $\alpha_1$  species. We conclude that  $\hat{\tilde{X}}_0 |\Psi_{gL}\rangle = 0$ . Therefore, we can view  $\hat{\tilde{X}}_0$  (and  $\hat{Y}_0$ ) as “emergent” guiding center coordinates and the generalized Laughlin state on the plane being their eigenstate with eigenvalue 0.